Modification and characterization of potential bioelectronic interfaces

Kyrylo Greben

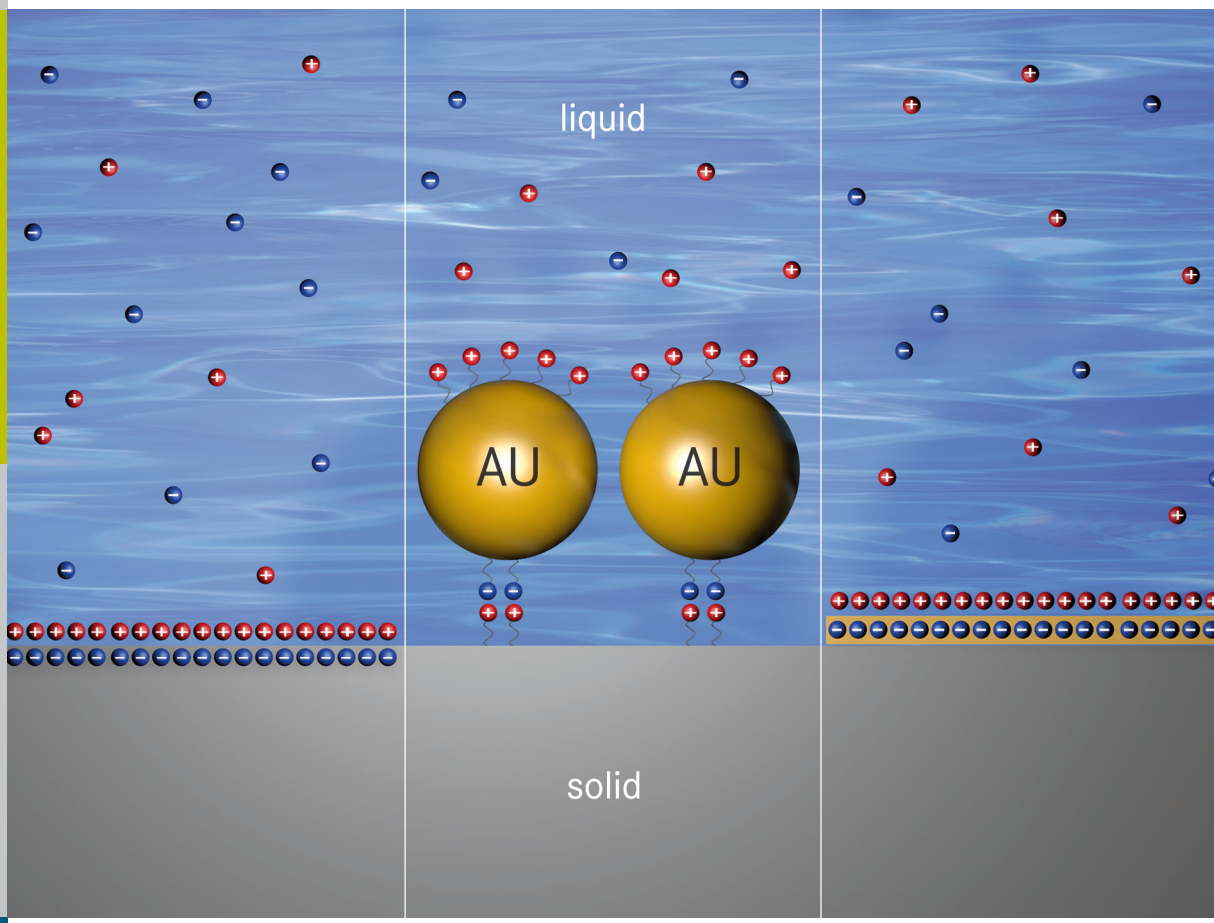

Member of the Helmholtz Association

Schlüsseltechnologien / Key Technologies
Band / Volume 101
ISBN 978-3-95806-028-9

JÜLICH
FORSCHUNGSZENTRUM

Schriften des Forschungszentrums Jülich
Reihe Schlüsseltechnologien / Key Technologies Band / Volume 101

Forschungszentrum Jülich GmbH
Peter Grünberg Institute / Institute of Complex Systems
Bioelectronics (PGI-8 / ICS-8)

Modification and characterization of potential bioelectronic interfaces

Kyrylo Greben

Schriften des Forschungszentrums Jülich
Reihe Schlüsseltechnologien / Key Technologies Band / Volume 101

ISSN 1866-1807 ISBN 978-3-95806-028-9

Bibliographic information published by the Deutsche Nationalbibliothek.
The Deutsche Nationalbibliothek lists this publication in the Deutsche
Nationalbibliografie; detailed bibliographic data are available in the
Internet at http://dnb.d-nb.de.

Publisher and Distributor:	Forschungszentrum Jülich GmbH Zentralbibliothek 52425 Jülich Tel: +49 2461 61-5368 Fax: +49 2461 61-6103 Email: zb-publikation@fz-juelich.de www.fz-juelich.de/zb
Cover Design:	Grafische Medien, Forschungszentrum Jülich GmbH
Printer:	Grafische Medien, Forschungszentrum Jülich GmbH
Copyright:	Forschungszentrum Jülich 2015

Schriften des Forschungszentrums Jülich
Reihe Schlüsseltechnologien / Key Technologies, Band / Volume 101

D 38 (Diss., Köln, Univ., 2015)

ISSN 1866-1807
ISBN 978-3-95806-028-9

The complete volume is freely available on the Internet on the Jülicher Open Access Server (JuSER)
at www.fz-juelich.de/zb/openaccess.

Zusammenfassung

In dieser Dissertation werden ebene, biokompatible dielektrische und metallische Oberflächen untersucht, die unter anderem mit selbstorganisierenden Monoschichten und funktionalisierten Gold-Nanopartikeln modifiziert werden.

Die Adhäsion und die Führung von Zellen (namentlich Neuronen) auf Substraten sind wichtige, und herausfordernde Aspekte der Bioelektronik. Die Optimierung und Modifizierung der Substrateigenschaften kann den Kontakt zwischen Zellen und Oberflächen sowie die Signalübertragung und Überlebensrate der Zellen potentiell verbessern. Heutzutage ist klar, dass Zellen über Proteine mit der Umgebung wechselwirken. Im Rahmen physikalischer Betrachtung bedeutet dies eine elektrostatische Wechselwirkung. Allerdings sind die Proteine (die für die Zelladhäsion verantwortlich sind) und die Mehrheit der anorganischen Substrate in Wasserlösungen negativ geladen. Dies führt zu elektrostatischer Abstoßung und beeinträchtigt dementsprechend die Adhäsion.

Die Benutzung funktionalisierter anorganischer Nanopartikel erlaubt die Modifizierung der Oberflächeneigenschaften verschiedener Materialien und verfeinert die Zelladhäsion. Darauf aufbauend sind in dieser Dissertation ebene, biokompatible dielektrische und metallische Oberflächen untersucht worden, die mit organischen Molekülen und funktionalisierten Gold Nanopartikeln modifiziert wurden. Als Messmethode diente eine optimierte Analyse des Oberflächenpotentials in Kombination mit unterschiedlichen Hilfsmethoden (z.B. Ellipsometrie, Wasser-Kontaktwinkelmessungen und Rasterelektronenmikroskopie). Außerdem wurde die Beschichtungsanlage für die molekularen Schichten, inklusive einer in-situ Reinigung und Aktivierung sowie einer elektronischen in-situ Analyse durch Kapazitiv- und Mikrowellenmessungen, entwickelt und getestet. Während dieser Arbeit sind die Beschichtungs- und Funktionalisierungsprozesse von Gold-Nanopartikeln sowie die Strömungspotential/Strömungsstrom Experimente für die Analyse des Oberflächenpotentials von Substraten und Schichten verbessert und optimiert worden.

Mit Hilfe unserer pH- und zeitabhängigen Analyse des ζ Potentials, können wir die unterschiedlichen Typen „einfacher" (z.B. verschiedene biokompatible Substrate, metallische Schichten, Graphen) und komplexer (z.B. Molekulare Schichten, funktionalisierte Gold Nanopartikel) Grenzflächen untersuchen. Für die Modifizierung von Oberflächen können wir außerdem die geeignetsten Kandidaten entsprechend ihrer Oberflächenladungen (z.B. organische Moleküle mit unterschiedlichen funktionalen Gruppen) bestimmen. Unsere weit gefächerte Analyse erlaubt die Stabilität der gegebenen Oberfläche zu bestimmen und die Veränderung des Oberflächenpotentials aufgrund von Oberflächenmodifizierungen (z.B. Beschichtung von Gold Nanopartikeln) zu überwachen.

Abstract

In this dissertation, planar biocompatible dielectric and metal surfaces, modified with self-assembling organic monolayers and functionalized gold nanoparticles are studied.

In the field of bioelectronics, adhesion and guiding of cells (especially neurons) on a substrate is of great importance, and withal a hard challenge. Optimization and engineering of properties of a carrier (biocompatible inorganic substrates) can potentially improve the contact between cells and substrates, increase the survival rate of cells and improve the signal transfer. Nowadays it is clear, that the cell interacts with outer world via proteins, which, following the physical approach, interact with the surface via electrostatic interaction. Unfortunately, in aqueous environment, proteins responsible for the cell adhesion as well as most inorganic substrates bear a net negative surface charge that leads to an electrostatic repulsion and, consequently, impairs adhesion.

The use of functionalized organic molecules or inorganic nanoparticles allows engineering the surface properties of various materials in order to facilitate the cell adhesion. Therefore, in this dissertation, planar biocompatible dielectric and metal surfaces modified subsequently with organic molecules, and functionalized gold nanoparticles are characterized via an optimized surface potential analysis in combination with other supporting techniques (e.g. ellipsometry, wetting angle and SEM). Additionally, a setup for the deposition of molecular monolayers, including in-situ cleaning and activation, accompanied by in-situ electronic analysis via capacitive and microwave measurements is developed and tested. During this work, the deposition and functionalization of AuNPs as well as a streaming potential/streaming current experiment for the analysis of the surface potential of the substrates and layers were improved and optimized.

Using especially the time- and pH-dependent analysis of the ζ potential, we can analyze the various types of 'simple' (e.g. various biocompatible substrates, metallic layers, graphene) and complex (e.g. molecular monolayers, functionalized gold nanoparticles) interfaces and identify possible candidates for the modification of a given surface with respect to their surface potential (e.g. organic molecules with different functionalization). Finally, our extended analysis allows us to determine the stability of a given surface and monitor the change of the surface potential due to the engineering of a surface (e.g. via deposition of gold nanoparticles).

Contents

I. Introduction

The properties of the surface represent maybe the most important constrain for the formation of any type of sample on the surface. This holds for inorganic (e.g. thin films), organic (e.g. molecular layers) as well as biological (e.g. cells) samples. Generally, *surface* is a discontinuity that terminates a phase. The phase may terminate at a vacuum or at the surface of another phase. The latter is also called an *interface*. An "ideal" or "free" surface is the interface between a solid or liquid and vacuum. Such a surface can be represented by a *surface energy*, which is a measure of the capacity of unsatisfied bonds of the surface (Figure 1).

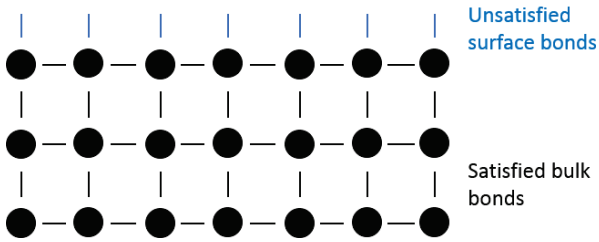

Figure 1: Schematic representation of the unsatisfied bonding capacity at a free surface (Adapted from: [1]).

At molecular scale, the *adhesion* of any species to the surface strongly depends on the surface properties of the substrate and is defined by the bonding capacity (i.e. surface energy). Independently of the type of an atom or molecule, each adhesion event has to lead to reduction of the free energy of the surface. Obviously not all incoming atoms or molecules fulfill this condition. Therefore, the chemical composition and structure of the substrate's surface play a major role in inorganic thin film growth. Typically, the first "layer" deposited on the surface is different from the subsequent layers. Moreover, it defines the growth mode, phase, and further properties of the rest of the film. For example, films of superconducting cuprate always start with a first layer of copper oxide that is then followed up by a complex Perovskite structure. Another example is the interfacial layer in $SrTiO_3/LaAlO_3$ systems. Depending on the combination of oxide layers at the interface (i.e. TiO_2/LaO or SrO/AlO_2), the interface can be either isolating or conducting.

In recent years, a growing attention for the adhesion of biological material to inorganic substrates is observed. This, among others, is triggered by potential bioelectronic applications. Moreover, biological active agents such as organic molecules or cells (esp. neuronal cells) are of interest not only in biomedical sciences but also in chemistry and physics. In case of biological material adhesion to inorganic substrates, the general term *biocompatibility* is used. It describes, for instance, the blood compatibility,

thromboresistance, tissue compatibility, foreign body reaction, protein adsorption, hemolysis, tissue ingrowth or adhesion to inorganic materials, etc. In general, organic/inorganic interfaces represent a wide field for possible applications in *molecular electronics* and *bioelectronics*. Moreover, the use of organic molecules or other biologically active agents allows engineering the surface properties of various materials.

Finally, adhesion of tissue cells to *biomaterials* is an important starting point for the successful incorporation of implants or the colonization of scaffolds for tissue engineering. Although the dominating role of protein adsorption in the regulation of cell adhesion has been identified, it is still not completely understood how cells perceive information on the characteristics of the substrate through the 'translation' by the protein overlay readily formed in any bio fluid [2].

Let us consider the field of *bioelectronics* in more details. Problems like the adhesion of the cell to the surface or guided growth of cells are of huge importance in this field. The main building blocks in bioelectronic circuits consist of neuronal cells that convert electro-chemical signals to an electronic circuit (reading) or vice versa, react on an electric stimulus of an electronic circuit (writing). The signal transfer rate between an inorganic electronic circuit and an organic neuronal cell represents one of the major challenges in bioelectronics, since most of the signal is lost due to bad contact, bad cell adhesion or good electric isolation between cell and electronic circuit. As examples, two typical representatives of bioelectronic devices are sketched in Figure 2, i.e. the ion-sensitive field effect transistor (ISFET) and the multi-electrode array (MEA). It is obvious that the better is the adhesion of the object to the surface and the better is the electronic signal transfer, the more sensible is the bioelectronic device.

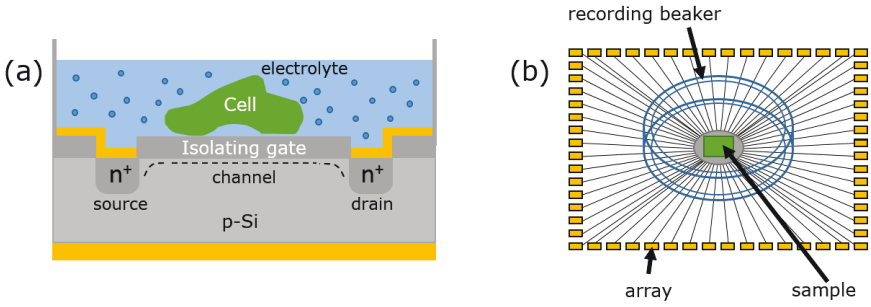

Figure 2: The schematic example of bioelectronic devices: a) ion-sensitive field effect transistor (ISFET) and b) multi-electrode array (MEA).

Cell adhesion is primarily a surface, biophysical phenomenon. Extensive developments in surface chemistry and physics of recent years provide a powerful and coherent approach for investigation of this phenomenon. The structural nature of the cell surface and its precise chemical composition determine the type of adhesion that is formed. Conversely, examination of the exact chemical conditions that affect the adhesion can help clarifying the structure and composition of the cell surface. There are different cell

adhesion mechanisms that are discussed nowadays [3]. They all can be simply divided into:

- *Chemical* [4]–[6],
- *Topographical* [7], [8],
- Purely *biological* (e.g. "lock-and-key") and
- *Physical* mechanisms.

The latter is mainly represented by *electrostatic interaction* between the cell membrane and the substrate's surface. The cell adhesion phenomena was already treated like a physical interaction, for example, in [9]. However, earlier, the adhesion of biomaterial was discussed in [1], where the approach, which is used is definitely physical and the cell-surface interactions are divided into molecular, protein, cell and tissue levels. Although, nowadays there are studies of the biomaterial adhesion at the molecular level [10], [11], it is already clear, that the cell interacts with the outer world via proteins. Therefore, the cell adhesion phenomena literally means protein-surface adhesion. There are special proteins, e.g. integrin, that are responsible for the cell adhesion. On one hand, these proteins possess a negative charge and, consequently, most living cells bear a net negative charge that leads to a mutual repulsive cell-cell interaction and contact between cells requires the formation of thin microvilli by at least one cell to overcome this barrier. On the other hand, cell adhesion might occur due to electrodynamic attraction, since, in particular, positively charged domains of peptides can promote the adhesion of proteins, bacteria [12], [13] and neuronal cells [14]. This finding was supported by the observation that positive charges associated with surface-bound, synthetic molecules containing amino groups can also promote the adhesion and growth of neurons [15]–[18].

Electrostatic interaction can also arise between charged proteins or a cell and a surface. In aqueous solution, essentially all interfaces carry electrically charged groups. The charge may originate from

- Association or dissociation of surface groups. This applies if ionizable groups are at the surface (e.g. carboxyl, amino, imidazole, and phosphate). For synthetic materials (e.g. polymers), the type of charged groups can be chosen by controlling the preparation conditions.
- Specific adsorption of ions from solution. This implies that the adsorption forces are (partly) of non-electric nature so that the ions can overcome and create a net electrostatic potential. Well-known examples of specifically adsorbing ions are ionic surfactants or light ions (e.g. K^+, Na^+, Cl^-).

From above-mentioned arguments, it is already obvious that in order to control and manipulate the growth of inorganic, organic and biological samples, it is essential to control and, if possible, tailor the surface of the carrier. One important aspect, for instance, for the adhesion of biological objects to an inorganic surface for bioelectronic applications, is the analysis and, if necessary, modification of the surface charge of a

carrier (substrate) under conditions that are identical or at least comparable to the conditions used during deposition or immobilization of the biomaterial.

The latter represents the one of the main *motivations* for the current dissertation, i.e. the investigation and possible optimization of inorganic surfaces for potential bioelectronic applications. Since there are different strategies of interfacing cells, the *focus* of this work lies on the impact of *electrostatic cell adhesion*. For this purpose, the surfaces are modified subsequently with bioactive agents such as organic molecules, and functionalized inorganic nanoparticles using and the surface potential characterization of planar biocompatible dielectric or metal surfaces in aqueous solution is developed, optimized and used as one of a number of techniques to characterize abovementioned complex interfaces.

II. Theoretical background

The discovery of electrokinetic phenomena by Reuss in 1808 and further investigations that gave rise to the concept of the electrical double layer (see Section II.1) have played an important role in understanding of colloidal stability at that time. Nowadays, they are widely used for investigation of different types of systems ranging from colloidal particles in the suspension to complex interfaces containing biological objects. *Electrokinetic phenomena* are a family of effects in which a liquid moves tangentially to a charged surface. Well-known phenomena of this kind are electrophoresis (when charged particles move in the applied electric field), electro-osmosis (when liquid moves under the influence of applied potential), streaming potential (arises on the surface when liquid moves adjacent to it), and sedimentation potential (arising from the movement of charged particles under the gravitation). All these phenomena are sketched in Section II.3, where we will also go into details about how to evaluate the surface charge using streaming potential/streaming current phenomena. In Section II.2, the origins of surface charges in aqueous electrolyte solutions are discussed from the point of view of chemistry of given surfaces. Sections II.1 and II.2 give a basic introduction to the electrical phenomena at interfaces.

II.1 Electrical double layer

In the contact with a polar medium (e.g. water), the majority of surfaces show a definite *surface charge* as a consequence of ionization, ionic adsorption and ionic dissolution. This surface charge influences the arrangement of neighboring ions in the polar medium. Ions of opposite sign will be attracted to the surface and ions of equal sign will be repelled. Due to mixing, as a consequence of thermic movements and Brown's movement, an electrical double layer (EDL) is formed (see Figure 3).

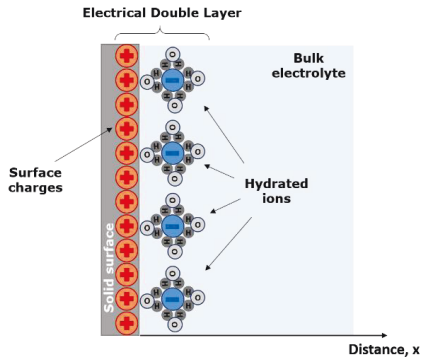

Figure 3: A simple model of an electrical double layer formed near the surface. The surface, for instance, is positively charged, negative ions are attracted to the surface and positive ions are repelled.

This double layer consists of a charged surface and a neutralized surplus of equally but oppositely charged ions diffusely spread through the polar medium. The double layer is characterized by the ion arrangement and the magnitude of the electrical potential near the charged surface.

II.1.1 Quincke - Helmholtz - Smoluchowski

Historically, Georg Quincke was the first, who proposed the idea of the EDL around 1860. He performed extensive investigations of streaming potential, electroosmosis and other, at that time known, electrokinetic phenomena. These discoveries led him to postulate the idea of a space charge that exists outside a charged surface and has a charge opposite to that on the surface. The existence of this space charge was necessary for Quincke to explain qualitatively both the electroosmosis and the streaming potential. Quincke's introduction of the space charge was of crucial importance for colloid science because it meant the discovery of the EDL. This concept is indispensable for modern treatment of colloidal stability [19].

In 1879, Hermann von Helmholtz derived a quantitative theory for electrokinetic phenomena based on Quincke's idea of EDLs. He published a paper entitled "Studien über elektrische Grenzschichten", in which he formulated a theory for electroosmosis and derived an equation, which described the connection between the electroosmosis in a tube and the electrical potential on the inner surface of the tube.

At that time, it was assumed that a capillary contains a net space charge, which starts to move if an electric field is applied and which entrains the liquid into which it is embedded, to demonstrate the electroosmotic volume flow Q_{eo}. Neither the origin of these charges was clear, nor were there concrete suggestions about the charge distribution. Even the question whether the double layer was as a whole electroneutral or not, was under dispute until eventually the issue was decided in favor of electroneutrality.

Later Helmholtz assumed that the classical hydrodynamic equations would also apply to double layer region, i.e. that the flow is laminar and only parallel to the surface and that the applied potential can simply be superimposed to that of the EDL. These assumptions are nowadays considered to be justified for regular conditions, but at that time, their applicability was not obvious.

Helmholtz's derivations essentially coincide with the present-day ones, i.e. at each position the viscous resistance is equal to the electric force:

$$\eta \nabla^2 v = E\rho, \tag{1}$$

where η is the viscosity, v is the flow speed and ρ is the electric charge density of the volume element where E, the electric field, is applied. The potential ψ was introduced via Poisson's equation:

$$\nabla^2\psi = -\rho/\varepsilon\varepsilon_0, \tag{2}$$

where ε is the relative dielectric constant and ε_0 is a vacuum permittivity. Integration over the surface area of the potential eventually yielded the potential difference:

$$\Delta\psi = \psi(\text{at the wall}) - \psi(\text{interior of capillary}). \tag{3}$$

It should be noted that the approach is very similar to the one used to date, except the surface potential $\Delta\psi$ being replaced by the zeta potential ζ, that characterizes the potential at the shear plane. With all of the more recent reinterpretation, the Helmholtz equation for electroosmosis finally yields:

$$Q_{eo} = -\frac{\varepsilon\varepsilon_0\rho I}{\eta K^L} \tag{4}$$

where I is the current density and K^L is the specific conductivity of the bulk liquid.

This equation has the same form as the well-known Smoluchowski equation, except that Helmholtz neglected the relative dielectric constant. He took $\varepsilon = 1$. Helmholtz published his theory in 1879 and Smoluchowski published an improved version in 1903.

II.1.2 Gouy-Chapman model

Louis-Georges Gouy developed his theory for a double layer that includes a diffuse space charge in 1910. David Leonard Chapman independently formulated an equivalent theory in 1913.

Both, Gouy and Chapman used the Poisson equation to describe the electrostatic attraction of counterions to a surface and the Boltzmann relation to describe the statistical tendency of the counterions to diffuse away from a region of high concentration.

In the resulting Gouy-Chapman theory, the potential of the mean force in the Poisson-Boltzmann equation is replaced by the mean electrostatic potential energy, and all ion-ion correlations in the EDL are ignored except for the effect of the mean potential. The

following assumptions have been used: (a) the surface is planar, infinite and uniformly charged, (b) ions in the diffuse part carry a unit charge, (c) the polar medium effects the double layer only through its dielectric constant which is unchanged over the whole diffuse part of the layer, and (d) the polar medium has the characteristics of a symmetrical electrolyte. Thus, this model describes the relation between charge, potential and electrolyte concentration, neglecting the ion size. Additionally, ions are regarded as hard spheres with embedded point charges, and water is referred to as a structureless medium.

The structure of the more distant diffuse layer is determined by electrostatic interactions described by the Gouy–Chapman theory. The electric potential profile within the diffuse layer can be obtained from the Poisson equation, which describes the potential–charge relationship, and the Boltzmann law, which determines the distribution of ions in an electric field [20]:

$$\nabla^2\Psi = -\frac{\rho}{\varepsilon\varepsilon_0} = -\frac{e}{\varepsilon\varepsilon_0}\sum_i z_i n_{i\infty} \exp\left(\frac{z_i e\Psi}{kT}\right), \tag{5}$$

where $\rho = \sum_i e\, z_i n_i$ is the electric charge density of ions of valence z_i, n_i - the number concentration accumulated within the diffuse layer, Ψ represents the local electric potential and ε is the dielectric permittivity of the medium. In the absence of specific adsorption of ions (later introduced by Stern), the diffuse layer charge is equal to the surface charge σ^0. Taking into account boundary conditions, i.e. the potential Ψ^0 at the surface and the potential in the bulk $\Psi^B = 0$, we obtain:

$$\frac{\partial\Psi}{\partial n} = -\frac{\sigma}{\varepsilon\varepsilon_0}, \tag{6}$$

where n is the normal at the particle surface pointing into the liquid.

If the potential is low, i.e.:

$$\left|\frac{z_i e\Psi}{kT}\right| \ll 1, \tag{7}$$

equation (5) reduces to the linearized Poisson-Boltzmann equation (Debye-Hückel equation):

$$\Delta\Psi = \kappa^2\Psi. \tag{8}$$

The Gouy–Chapman model for the diffuse layer gave rise to a very important parameter κ, which characterizes the thickness of the diffuse layer:

$$\kappa = \left[\frac{1}{\varepsilon\varepsilon_0 kT}\sum_i e^2 z_i^2 n_{i\infty}\right]^{1/2} \quad (9)$$

Here $n_{i\infty}$ is the bulk concentration of the ith ion in the bulk phase and z_i is its valence. κ^{-1} has dimensions of a length and is called the *Debye length*. It has a fundamental importance in the theory for electrokinetic phenomena and is usually used in combination with the particle radius a as κa.

Interestingly, Smoluchowski mentioned Gouy's theory in a footnote but seemed not to have utilize this knowledge.

II.1.3 Gouy-Chapman-Stern-Graham model

Actually, the Gouy-Chapman model fails for highly charged double layers. In 1924, Otto Stern suggested to combine the Helmholtz-Smoluchowski's theory with the Gouy-Chapman's one. In Stern's model, some ions adhere to the electrode as suggested by Helmholtz, defining an internal *Stern layer*, while some form a *Gouy-Chapman diffuse layer*. The Stern layer is the innermost non-diffuse part of the counter layer, which may contain adsorbed ions. The diffuse layer is generic while the Stern layer strongly depends on the nature of the substances involved. In principle, Stern noticed the drawback of neglecting the ion size and therefore proposed a model, which starts from the following assumptions: (a) ions possess a finite size, (b) they cannot approach the surface to a distance smaller than the magnitude of ionic radius and (c) the possibility of specific ion adsorption exists.

According to the Stern model, the charge is given by:

$$\sigma = \sigma_s + \sigma_g \quad (10)$$

where σ_g is the charge given by Gouy's model, while σ_s is the charge of the Stern layer.

The electric field within the Stern layer can reach a very high strength, which results in a modification of the behavior of species (ions, adsorbate, and solvent molecules) that build up this layer. Processes that can occur within this compact layer are regulated by short-range specific interactions. The electric state of the Stern layer is determined by properties of the solvent (dielectric permittivity), the degree of ionization of the surface group and/or specific adsorption of species from the solution. Charge formation

processes within the Stern layer may proceed at various rates, which, in some cases, may lead to time-dependent effects.

Finally, David C. Grahame modified Stern's model in 1947 [21]. He proposed that some ionic or uncharged species could penetrate the Stern layer, although solvent molecules normally occupy the closest approach to the electrode. This could occur if ions lose their solvation shell as they approach the electrode. Under the impact of electrostatic and/or van der Waals forces ions adsorb on the surfaces and overcome the effect of thermal movements. They are called specifically adsorbed ions. Thus, this model proposed the existence of three regions (see Figure 4). The *inner Helmholtz plane (IHP)* passes through the centers of the specifically adsorbed ions. The *outer Helmholtz plane (OHP)* passes through the centers of solvated ions at the distance of their closest approach to the electrode. Finally, the diffuse layer is the region beyond the OHP, which starts at the shear plane.

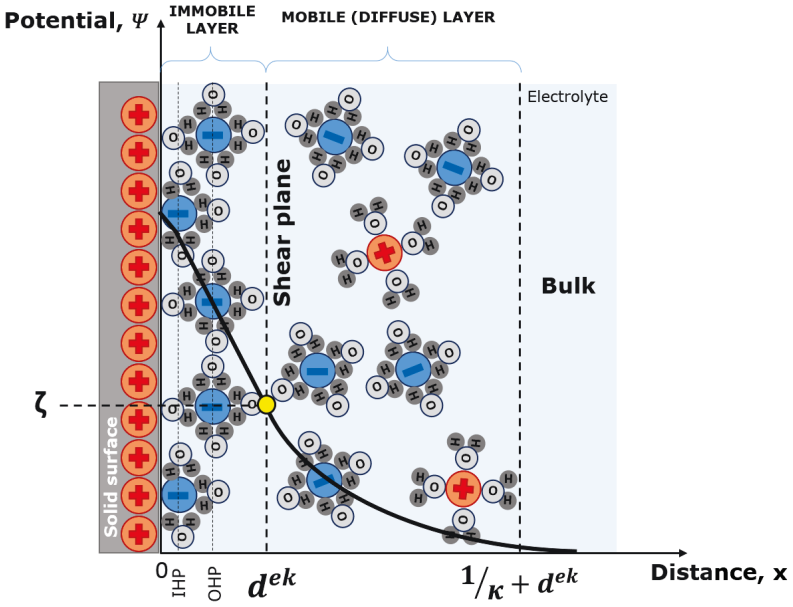

Figure 4: Schematic structure of the electrical double layer (EDL), according the Gouy-Chapman-Stern-Grahame (GCSG) theory.

The charge of the surface (x=0) is partially compensated by the association of charged groups with counterions of the opposite charge located at the IHP at distance β, defining the potential Ψ^i. The potential Ψ^d at the OHP (d-plane) is the potential at the beginning of the diffuse part of the double layer. It is usually assumed that hydrodynamic flow vanishes at a finite distance from the solid surface. The plane separating the liquid into immobile and mobile regions is called the electrokinetic slip plane (or shear plane). Within the diffuse layer, the potential at this d^{ek}-plane is determined as the electrokinetic or *ζ-potential*, which divides the stagnant from the mobile part of the diffuse layer [22].

Generally, its separation from the d-plane is typically of the order of ~1-1.5 nm. The thickness of the diffuse part of the electrical interfacial layer (Debye length) for water, NaCl (10^{-3} M), and Na_2SO_4 (10^{-3} M) at 25 °C are ~961.8, ~9.6, and ~6.1 nm, respectively, depending on the electrolyte and its concentration as well. The *ζ potential* characterizes the property of both surface and electrolyte and is widely used in colloid chemistry for characterization of the behavior of dispersive systems in liquids [23]. The earliest use of the notation 'ζ potential' was found in the book by Herbert Freundlich, entitled "Kapillarchemie" (second edition), published in 1922 [19]. Freundlich's book on surface and colloid science was widely used and considered as a reliable source of information. The general use of the symbol ζ for the electrical potential at the slip plane is probably derived from his book.

In conclusion, the surface (i.e. wall) potential Ψ^0 and the surface charge density σ^0 (see figure 4), cannot be determined experimentally. However, the potential at the shear plane, the ζ potential, can be measured by electrokinetic methods. The electrokinetic or ζ potential is frequently assumed to be equal to that at the boundary between the Stern and the diffuse layer (i.e. at the OHP):

$$\zeta \approx \Psi^d. \tag{11}$$

In the Stern layer the potential changes linear with the distance x, whereas in the Gouy-Chapman layer it varies exponentially with x:

$$\Psi(x) = \Psi_d e^{-\kappa(x-d)}, \tag{12}$$

where x is the distance, d the thickness of the Stern layer and κ^{-1} is the Debye length.

Additionally, the surface charge at the distance d is given by:

$$\sigma_d = (\varepsilon\varepsilon_0 nkT)^{1/2} \sinh\left(\frac{Ze\Psi_d}{2kT}\right). \tag{13}$$

II.1.4 Isoelectric point, point of zero charge

A scientist with a good insight into the charging process of colloids was the Englishman William Hardy, a physiologist working with biological systems such as proteins. In a paper from 1905, on globulins produced from oxblood serum, he coined the word *isoelectric point* and defined it as the pH value where the amounts of positive and negative electrokinetic charge on a colloidal particle are the same.

The net electrokinetic charge is affected by the pH of its surrounding environment and depends on the loss or gain of protons (H^+). Under the usual conditions, the surface-charge-determining ions are H^+ and OH^-. Therefore, the net surface charge is affected by the pH of the liquid in which the solid is submerged. Practically, the isoelectric point defines the pH at which the ζ potential equals zero.

However, one has to clearly distinguish between the *isoelectric point* and the *point of zero charge*. The isoelectric point corresponds to the electrical charge σ^{ek} (electrokinetic charge at the slip plane) at certain pH value. As discussed in previous sections the Stern layer consists of specifically adsorbed ions, which give rise to the charge σ^{d} at the outer Helmholtz plane. There are many discussions between physicists and chemists about whether $\sigma^{ek} = \sigma^{d}$. However, for many practical applications this assumption seems to be valid [24].

Finally, the *point of zero charge* would refer to the charge σ^0 right at the surface, which usually is larger compared to σ^{ek}. Although, the point of zero charge cannot be detected by standard electrokinetic measurements, it is typically done via potentiometric titration method.

II.2 Origins of Surface Charge

As mentioned in previous sections, interfaces between solids and liquids carry an electric charge. There are many origins of this surface charge depending upon the nature of the surface and its surrounding medium. Here we will consider the most important mechanisms.

According to Lyklema [25], [26], the origin of charges at interfaces may be attributed to

(i) the dissociation of surface groups,
(ii) the preferential adsorption of cations or anions,
(iii) the adsorption of polyelectrolytes,
(iv) the isomorphic substitution of cations and anions, and
(v) the accumulation or depletion of electrons (i.e. due to an applied potential).

Since anions are preferentially adsorbed in a neutral 1:1-electrolyte solution, the ζ potential of most surfaces is negative. Some of the most prominent mechanisms are discussed below.

II.2.1 Ionization of surface groups

Ionization (dissociation) of acidic groups on the solid surface gives rise to a negatively charged surface [27]. Conversely, a basic surface will take on a positive charge. Both of these situations are shown schematically in Figure 5. In both cases, the magnitude of the surface charge depends on the acidic or basic strengths of the surface groups and on pH of the solution. The surface charge can be reduced to zero by suppressing the surface ionization by decreasing the pH of the electrolyte in case of negatively charged surfaces (Figure 5a) or by increasing the pH of the electrolyte in the case of positively charged surfaces (Figure 5b), respectively.

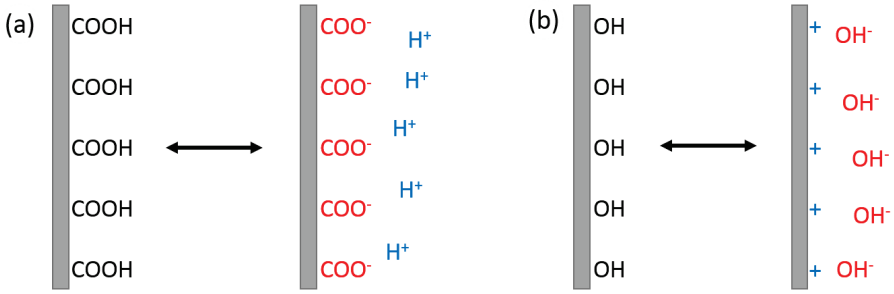

Figure 5: Origins of surface charge: dissociation of (a) acidic surface groups and (b) basic surface groups. Adapted from [28].

II.2.2 Differential loss of ions from the crystal lattice

As an example, a crystal of silver iodide placed in water is considered. Ions begin to dissolve in the electrolyte. If equal amounts of Ag^+ and I^- ions would dissolve, the surface would be uncharged. However, silver ions dissolve preferentially, leaving a negatively charged surface (Figure 6). If Ag^+ ions are added, the negative surface charge is reduced and finally becomes positive.

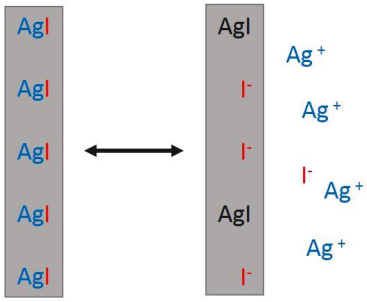

Figure 6: Origins of surface charge: differential loss of ions.

II.2.3 Adsorption of charged species (ions and ionic surfactants)

Charged species (ions or ionic surfactants) can be specifically adsorbed on a surface, leading, in the case of cationic surfactants, to a positively charged surface (Figure 7a) and, in the case of anionic surfactants, to a negatively charged surface (Figure 7b). Moreover, inorganic ions can interact with charged surfaces in one of two distinct ways:

(i) non-specific ion adsorption, where they have no effect on the isoelectric point and
(ii) specific ion adsorption, which will lead to a change of the isoelectric point.

The specific adsorption of ions onto a surface, even at low concentrations, can have a dramatic effect on the ζ potential. In some cases, specific ion adsorption can even lead to a charge reversal of the surface [29].

Generally, the extent of these processes depends on the chemical composition and physical structure of the solid and the composition of the surrounding liquid. Therefore, the formation of the EDL and the magnitude and sign of the ζ potential are determined by the combination of the solid and the liquid, i.e. the interface.

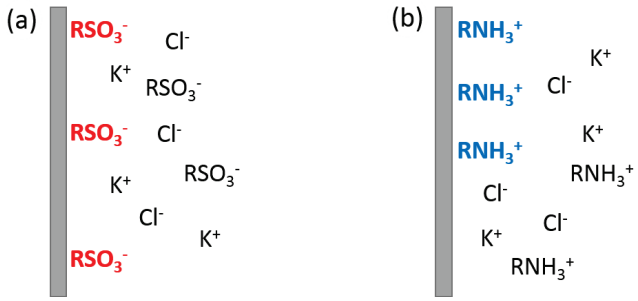

Figure 7: Origins of surface charge: ions and surfactants adsorption.

II.3 Methods to determine the ζ potential

The Gouy-Chapman-Stern-Grahame (GCSG) model shows that the ζ potential is a consequence of the construction of the double layer and that it is the measurable property of a charged interface. However, from the above it is clear that the ζ potential is not only property of the surface, but it is also changing according to the changes in the solution. Therefore, ζ potential measurements allow analyzing changes that take

place in the solution. This makes the measurement of the ζ potential an important aspect for analysis of many technical processes.

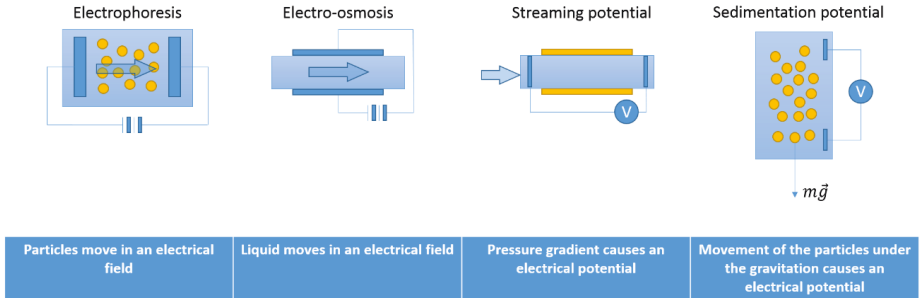

Figure 8: Classical electrokinetic phenomena.

Generally, the form of the solid/liquid interface determines the choice of the electrokinetic technique (see Figure 8) for the analysis of the ζ potential. For example, single particles in dilute colloidal systems are preferentially measured via electrophoresis or sedimentation potential measurements, whereas concentrated plugs of particles fixed in a defined volume are usually measured using streaming current or streaming potential, or alternatively electroosmosis techniques. For macroscopic surfaces of simple geometry (capillaries, channels, planar substrates) streaming current/streaming potential, electroosmosis are the best choice.

Electrokinetic equations that describe the motion of charged colloidal particles in a liquid electrolyte caused by an external electric field are based on a Navier-Stokes equation for liquid flow of ionic species and the Poisson equation connecting the electric potential with concentrations of ions. The Navier-Stokes equation for a liquid flow $\boldsymbol{u}(\boldsymbol{r})$ around a particle is given by:

$$\eta\nabla\times\nabla\times\boldsymbol{u}(\boldsymbol{r})+\nabla\mathrm{p}(\boldsymbol{r})+\rho_{el}(\boldsymbol{r})\nabla\psi(\boldsymbol{r})=0,\qquad r>a \tag{14}$$

where η is the viscosity of the electrolyte solution, $\mathrm{p}(\boldsymbol{r})$ is the pressure at position $\boldsymbol{r}$, $\rho_{el}(\boldsymbol{r})$ is the charge density resulting from the mobile charged ionic species, and $\psi(\boldsymbol{r})$is the electric potential.

All electrokinetic effects originate from two generic phenomena, namely, the electroosmotic flow and the convective electric surface current within the EDL. For non-conducting solids, Smoluchowski [30] derived equations for these generic phenomena, which allowed an extension of the theory to all other electrokinetic phenomena.

Electroosmosis is the oldest electrokinetic technique, discovered by Gustav Wiedemann in 1852 [19]. It represents a measurement of the flow of a liquid through a porous membrane in a known electrical field. The speed of electroosmotic flow is proportional

to interaction of the external electrical field with the charge of the liquid. Due to the potential difference of the two electrodes, electroosmosis causes a pressure gradient, which causes the flow of the liquid.

Electrophoresis appears when a fine (e.g., colloidal) dispersion of, for instance, dielectric matter in the electrolytic solution is exposed to an electrical field. Single dispersed particles are electrically charged in the dispersion medium and an EDL is formed around each of them. If the liquid phase as a whole is prevented from flowing in one direction, only charged particles will be kept in motion in the electrical field, and they will travel, depending on their charge and the electric field, towards the cathode or anode. The velocity of the particle with respect to a medium at rest is proportional to the ζ potential.

Sedimentation (Dorn) potential is the phenomenon opposite to the electrophoresis. It realizes during the movements of electrified particles in gravitational or sedimentation fields in centrifuges. This movement causes the potential difference between two electrodes, placed at a different level. This method is most rarely used to study the electrokinetic phenomena.

Finally, the *streaming potential* represents a phenomenon opposite to that of electroosmosis. The physicist Georg Quincke first reported about it in 1859, when he pumped water through a tube and measured an electrical potential difference between the ends of the tube. By mixing different materials, e.g. glass, sand, sulfur, talk, graphite, silk, linen, or ivory into the tube, he found that the magnitude of the potential difference varied for the different systems whereas the polarity of the potential was always the same. This latter results of course from the fact that many natural materials tend to be negatively charged in aqueous solution. He also discovered that the potential difference was independent of the cross section and the thickness of the channel and that the streaming potential varied linearly with the applied pressure. Amongst other important observations he found that addition of sodium chloride lowered the streaming potential [19].

Generally, the streaming potential arises when counter-ion displacement caused by hydrodynamic flow along a charged surface is balanced by a reverse conduction current that evolves due to a potential difference along a liquid stream. Let us consider a capillary with cross-section A and length L with charged walls. A pressure difference between the two ends of the capillary, Δp, is produced externally to drive the liquid through the capillary. Since the fluid near the interface carries an excess of charge equal to σ^{ek}, its motion will produce an electric current known as streaming current I_{str}

$$I_{str} = -\frac{\varepsilon\varepsilon_0\zeta}{\eta}\frac{A}{L}\Delta p \tag{15}$$

with η and ε representing the dynamic viscosity and the relative dielectric constant of the liquid, respectively. The current I_{str} can be recorded with measuring electrodes at

both ends of the capillary that are connected via a small external resistance (short-circuit conditions). If this resistance is large (open circuit), transport of ions by this current leads to the accumulation of charges of opposite signs between the two ends of the capillary and, consequently, to the appearance of a potential difference across the length of the capillary i.e. the streaming-potential U_{str}. This gives rise to a conduction current I_c:

$$I_c = K_L \frac{A}{L} U_{str} \tag{16}$$

The streaming-potential is then given by $I_{str} = I_c$, and is directly proportional to the ζ potential according to the equation:

$$\frac{U_{str}}{\Delta p} = \frac{\varepsilon \varepsilon_0 \zeta}{\eta K_L} \tag{17}$$

III. Experimental Techniques and Sample Preparation

For bioelectronic applications, it is important to use substrates such as glass or silicon that are as well suitable for the biological applications as compatible for electronic circuity. In this chapter, we describe the preparation techniques and steps that are used to modify the surfaces of given substrates, which include the cleaning routines (Section III.1), deposition of self-assembled molecular monolayers (SAMs) (Section III.2 and III.3), deposition of graphene layers (Section III.4) and the deposition and functionalization of gold nanoparticles (AuNPs) (Section III.5). Furthermore, in the second part, we briefly describe the characterization methods, which were used to control the quality of the molecular monolayers, such as ellipsometry (Section III.6.1) and contact angle measurements (Section III.6.2) and to analyze the surface potential of surfaces, namely streaming potential/streaming current experiments (Section III.6.3).

III.1 Cleaning and treatment of samples

In this work, we have mainly used commercial borosilicate glass substrates ("Praezisions Glas&Optik GmbH", Iserlohn, Germany) and p-doped silicon (Si (100) with 1-10Ω and Si (111), from the "CrysTec GmbH", Berlin, Germany). The latter possess 3nm native oxide and are thermally oxidized (Centrotherm LPCVD System E1200 R&D Furnace in clean room environment) to generate an extra 100nm thick SiO_2 layer on the surface. An additional advantage of these substrates is given by their low dielectric permittivity ε, which is compared to the permittivity of organic molecules [31] and allows microwave and capacitive spectroscopy to detect small changes in the signal due to the deposition of molecules. Furthermore, we used r-cut sapphire ("CrysTec GmbH", Berlin, Germany), as a reference substrate especially in the microwave experiments.

Since our work is focused on the surface properties, the cleaning of the sample surface turned to be a very important part of this work because the adhesion of SAMs to the surface depends strongly on the surface quality [32], [33]. Furthermore, the streaming potential method is extremely sensitive to any pollutant adsorbed on the surface (e.g. dust or adsorbed gasses). Therefore, two different protocols were used for the surface cleaning.

Protocol A: Substrates undergo a chemical cleaning procedure, which includes several steps:

1) Chemical cleaning in acetone for 3 minutes in an ultrasonic bath at 25°C with 100% power (320W) at 37kHz frequency, then

2) Cleaning in isopropyl alcohol (2-Propanol, > 99.8 %, KMF) in ultrasonic bath (for 3min at 25°C, 320W, 37kHz) and, finally,

3) Rinsing in double-distilled water and drying with nitrogen.

Alternatively, for special surface cleanliness, the samples were cleaned using the Protocol B in the cleanroom environment (class-10).

Protocol B: Steps 1) and 2) are identical to the Protocol A.

3) Rinsing in distilled water cascades for 5 minutes in pre-rinsing and 5 minutes in rinsing area (>12MΩ resistance).

4) Drying with nitrogen and 3 minutes soft baking at 120°C in order to remove the adsorbed water.

5) After the cleaning, if needed, the samples were put in the plastic container and laminated into the plastic foil in order to minimize the influence of the atmosphere.

For microwave and capacitive measurements reference substrates were patterned with microwave waveguide lines (different variations of coplanar and microstrip lines) and interdigitate capacitive structures respectively, using optical lithography and electron beam lithography in combination with lift-off technology. The protocol for optical lithography was as follows:

Spin-coating and baking: *(1) Spinning LOR3B / 2000rpm, (2) 6 min of soft baking at 180°C, (3) Spinning nLoff 2020 / 4000rpm and (4) 1min soft baking at 110°C.*

Exposure (for optical lithography): *3.5-4.4s (CP-mode, 305W), using a Cr mask with microwave structures and interdigitate electrode pattern.*

Development: *(1) Soft backing at 110°C for 1min, (2) Rinsing in MIF for 40-60 and (3) Rinsing in DI water for 5min*

Metallization: *different thicknesses of Au and Pt*

Lift-off: *using LOR3B remover or Acetone.*

The metallization step (evaporation as well as magnetron sputtering deposition) was not only used in the lift-off lithographical procedure, but was also applied to obtain metallic layers (typically Au, Pt or Cr).

III.2 Molecular layers

Due to of their various functionality, which is achieved via different functional groups, self-assembling monolayers (SAMs), as discussed in Section III.2.1, are often used for the modification of substrates. The deposition of SAMs onto the surface represents an important part of the sample preparation in present work. For preparation of silane SAMs on bioelectronic-suitable substrates, we used the physically separated process steps, which consisted of the sample cleaning (discussed in Section III.1), surface activation via oxygen plasma (Section III.2.2) and silanization through the gaseous phase (Section III.2.4) and will be discussed in following sections. Due to the difficulty caused by the separation of the different preparation steps, a *new device* was developed as the part of this work. It will be presented in the Section III.3.

III.2.1 Self-assembled monolayers

Structurally well-defined organic monolayers on solid surfaces allow experimentalists to simplify and model a large variety of interfacial phenomena that are often difficult to study at "natural" interfaces due to heterogeneous or poorly defined structure. Organic disulfides, thiols, and sulfides on gold surfaces and carboxylic acids and silanes on various oxide surfaces have been explored in recent years and widely used as model as well as surface active systems and also as molecules, stimulating cell adhesion. For example, SAMs of organosilanes have been successfully used to tailor material surfaces to obtain control over the molecular composition and the resulting integral properties of the surfaces [33]. Recent studies have used SAMs to evaluate the effect of surface charge, wettability and topography on protein adsorption and cell behavior using in vitro assay systems [2], [18], [34], [35]. The strength of cell adhesion and spreading on SAMs has been especially studied.

SAMs are ordered molecular assemblies that are formed spontaneously by the adsorption to the surface.

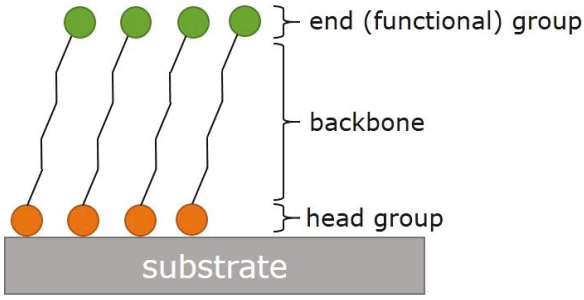

Figure 9: Schematic structure of self-assembling molecules.

The SAMs consist of a head group (Figure 9), which is chemisorbed to a specific substrate, the backbone, which can be a chain of isomers (typically alkyl chain), with a given length and an end or functional group, which can possess different functionalities, e.g. different by charge. The head group reacts with specific sites on the surface creating an attachment through a chemical bond. The energies associated with the chemisorption are of the order of hundred kJ/mol. Because of the exothermic interaction between substrate and head group, molecules try to occupy every available binding site on the surface. Chemisorption is very important, because only after molecules are put in place on the surface, formation of an ordered and closely packed assembly can start. The functional group determines the properties of the SAM surface, e.g. wettability and reactivity.

The most well-known and extensively studied SAMs are alkanethiols on gold. The high affinity of the thiol group to gold leads to a spontaneous formation of an Au–S bond. The formation of alkanethiols on gold is often presented as a model system of SAMs. Organosilanes can be used as a SAM system for hydroxylated substrates or substrates with a thin water layer. An appropriate substrate for the formation of silane SAMs is an oxidized silicon surface, which will be further discussed in the Section III.2.4. A variety of different substrates can be coated with silane SAMs such as Si-wafers, mica, PDMS, glass or even metals (e.g. Al with a top oxide layer), allowing for a Si-O bond. SAMs prepared on smooth surfaces like Si wafers exhibit extraordinary properties such as chemical homogeneity, ultra-low surface roughness and controlled wettability. The latter can be varied from hydrophilic to hydrophobic, depending on the end group of the silane. Silane layers in particular are mechanically robust, thermally stable up to at least 250°C and are not subject to swelling in the presence of solvents. These properties render silane-coated substrates ideal model surfaces to study a wide range of physical, chemical and biological phenomena such as adhesion, adsorption, friction or nanofluidics of thin liquid films. Technical applications also benefit from the unique properties of SAMs. They act, for example, as lubrication layers in micro-electro-mechanical-systems (MEMS) or as coatings in microfluidic devices. In addition, silane SAMs were applied for wetting driven self-assembly processes to fabricate surfaces with well-defined lyophobic and lyophilic patterns [32].

III.2.2 Activation of the surface

The oxygen plasma activation is probably the most crucial and important step in the process of surface modification by silanization. Not only the removal of organic residues is an important issue, but also, and more important, the oxygen plasma treatment results in an activation of the sample surface.

III.2.2.1 Activation of the silicon surface

When the silicon crystal is cut or cleaved, the bonds between neighboring atoms are broken, creating dangling bonds at the surface. The surface energy is lowered by reducing the number of dangling bonds by rebonding. Reconstructed silicon surfaces evolve for instance with surface dimers. The effect of the activation of the silicon surface lies in the reconstruction of the silanol surface bonds and leads to the increase of their quantity [36]. Schematically, this process is shown in Figure 10:

Figure 10: Silanol bonds reconstruction, due to e.g. activation via oxygen plasma. Adapted from [37].

The interaction of silicon surfaces with oxygen gas can lead to either production of a silicon oxide film on the surface (passive oxidation):

$$Si(s) + O_2 \rightarrow SiO_2 \tag{18}$$

or to etching of the surface (active oxidation):

$$Si(s) + O \rightarrow SiO \tag{19}$$

Which oxidation process takes place depends on surface temperature and oxygen pressure. Active oxidation dominates at high temperatures, while passive oxidation dominates at high oxygen pressures [37].

The cleaning effect of an oxygen treatment is the result of the oxidation of carbon in the organic species, whereas the activation of the surface is related to the oxidative effect. Generally, the oxidative effect is related to the electronegativity of the ion. The oxygen molecule O_2 has an oxidation state equal to zero. This also means that O_2 molecules are weak oxidants. However, atomic oxygen ions are very electronegative, which means that they are chemically very active. As pointed out above (see equation (19)), in order to achieve an active oxidation of a silicon surface, atomic oxygen is needed. Due to the ionization processes, an oxygen plasma generates a lot of atomic oxygen. A certain energy of the plasma is needed to overcome the binding energy between two oxygen ions in an oxygen molecule (5.12eV) and to produce two separate ions. Due to relatively high pressures, used for the plasma activation, the number of atomic oxygen ions is very high. The characteristic reaction that takes place during ionization is:

$$e + O_2 \rightarrow O^+ + O + 2e \ (E_{ap} = 18.69eV) \quad (20)$$

where E_{ap} is the appearance energy of the resulting species.

Figure 11 displays an image of the oxygen plasma generator that was used for the first experiments.

Figure 11: The oxygen plasma generator.

The Si samples were mounted on the sample holder inside the plasma generator, which subsequently is pumped down to 10^{-2} mbar. Then the vacuum chamber is filled with oxygen at a pressure of 1.4mbar. The plasma is ignited and stabilized to a power of 200W. The overall time of the oxidation process takes 3 minutes. After the time lapse, the chamber is evacuated and samples are taken out.

III.2.3 Silanization mechanism

As we already discussed in Section III.2.1, the head group of the molecule always has to be considered together with the surface to which this molecule is about to bind. Consequently, silanes are the molecules that form the silanol bond (Si-O-Si) at the surface. Typically, the head group of silanes is hydrated and easily undergoes a chemisorption on an activated surface that also possesses silanol bonds. Schematically, the silanization process is shown in Figure 12:

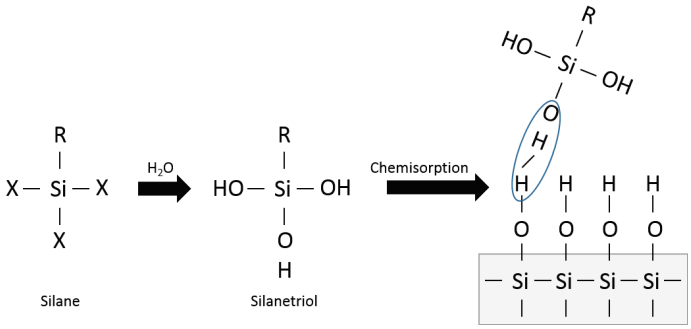

Figure 12: Silanization mechanism presented schematically.

From this figure, it is clear, that if the Si surface is not activated, which means it has less open bonds that are inhomogeneously distributed on the surface, the quality of the silanes deposition is poor and no monolayer coverage is expected.

III.2.4 Silanization process

Directly after a surface activation, samples are transferred into the Glove Box (Figure 13) for silanization process. The Glove Box is filled with an inert gas (Ar) at overpressure to prevent gasses of the atmosphere to enter.

Figure 13: The Glove Box.

As soon as the samples are transferred into the Glove Box, the silanization process starts. For this, a special desiccator is used. The samples are placed inside the desiccator

and the silane molecules are first filled into the syringe from the delivery beaker and then are poured out into the beaker inside the desiccator. Then the desiccator is closed and connected via a tube to a pump, which is located outside the Glove Box. Then the pressure inside the desiccator is reduced to a value, which depends on the vapor pressure of molecules that are to be silanized. For example, for APTES (3-aminopropyltriethoxysilane) molecules it equals to 5mbar. The desiccator is kept at that pressure for 1 hour before the silanization is finished.

In summary, the original protocol of SAMs preparation was as follows: the samples were cleaned in a chemical lab in one building. Then they were packed into the plastic container and transported into a laboratory in the other building where the oxygen plasma device is located. In this laboratory, samples were unpacked and mounted into the plasma generator for cleaning the sample surface from the organic species and activating the surface in order to facilitate the silanization quality. After the oxidation, samples were taken out of the plasma generator and were boxed again into the plastic container. Then, they were transported into again another laboratory, unpacked and placed into the desiccator inside the Glove Box for further silanization.

Obviously, this procedure has a number of drawbacks like long transportation time in the plastic container (reaction with the gas in the container and plastic container itself) and questionable reproducibility of the different steps at the different set-ups. We noticed that these effects affected the surface quality and consequently the SAMs monolayer quality seriously and, therefore, developed a device in which most process steps could be performed in-situ.

III.3 Deposition of molecular layers including in-situ characterization

In the Section III.2 we discussed the drawbacks of our standard silanization technique using different set-ups in different buildings. In order to overcome this problem, already Gilles [38] presented the CASINO concept (Cleaning and Silanization in One), which integrates the oxygen plasma generator, shown in Figure 11 with the desiccator that can be used for silanization.

In this chapter, an improved device concept (GLOBUS) will be discussed. It can be considered as a second generation of the CASINO device, however being the alone standing concept. The cumbersome and expensive microwave generator is replaced by a conventional microwave oven and various in-situ techniques for the characterization of the molecular layers are added. An overview of the different concept of the device is presented in Figure 14:

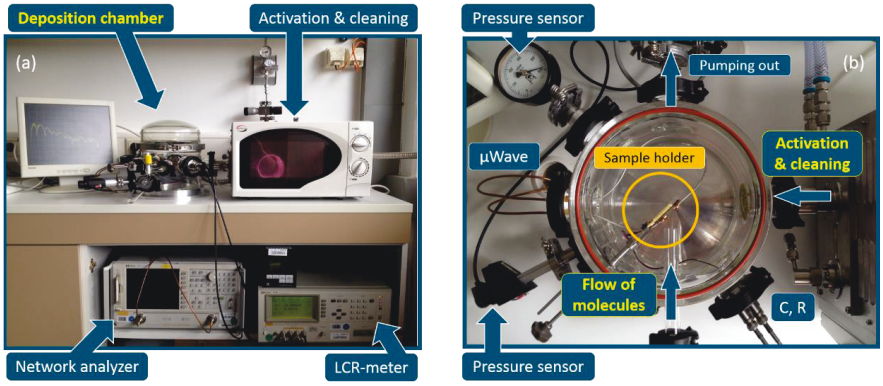

Figure 14: GLOBUS - The novel concept device for deposition of molecular monolayers, including in-situ cleaning and activation of substrates as well as in-situ electronic characterization of molecular monolayers: a) overview, b) top view.

III.3.1 Design and features

The CASINO device [38] proved that the general idea of combining cleaning and activation of substrates as well as deposition of molecular monolayers in one closed system works well. The GLOBUS device additionally allows monitoring the deposition of the molecular layers via in-situ electrical characterization (e.g. microwave and capacitive spectroscopy). Moreover, the deposition process can also be repeated when taking into account the possibility of removal of organic layers by applying activated oxygen for cleaning.

The main parts of the set-up are: (i) the glass recipient, containing various sample-holders, (ii) a conventional microwave oven for the generation of the activated oxygen, (iii) electronic measuring devices (e.g. network analyzer and LCR meter) that are read out via (iv) PC and (v) the pumping and ventilation system.

The working chamber is made completely of borosilicate glass in order to allow the visual control of the process. Evacuation pressure down to $3x10^{-2}$mbar is achieved via a vacuum pump including a fore vacuum pump, which is low enough for the evaporation of most molecules.

Samples mounted at the central position of the recipient can be cleaned, activated and characterized during deposition and until the surface is completely modified. This ensures minimization of contamination from the environment and a better reproducibility of the measurement.

The samples are placed in a combination of sample-holders, which consists of at least two parts. One is a movable and rotatable holder, which allows an ideal positioning of

the sample in front of the flow of molecules and activated oxygen, both impinging at 45° incidence angle on the substrate (Figure 14b). The second part (see Figure 15) represents the customized sample-holder for the electronic characterization of reference samples.

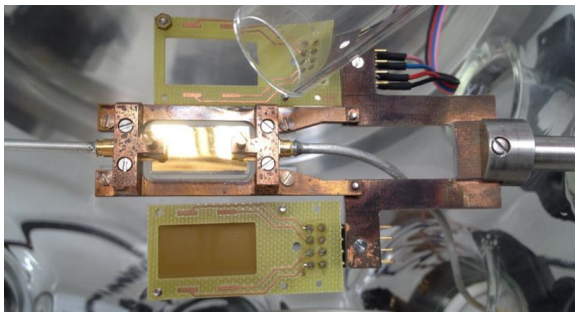

Figure 15: The design of the sample holder used for electronic characterization inside the GLOBUS device.

It has the special custom-made part for resistive, microwave (Figure 15-Figure 16), capacitive or surface acoustic waves analysis, respectively.

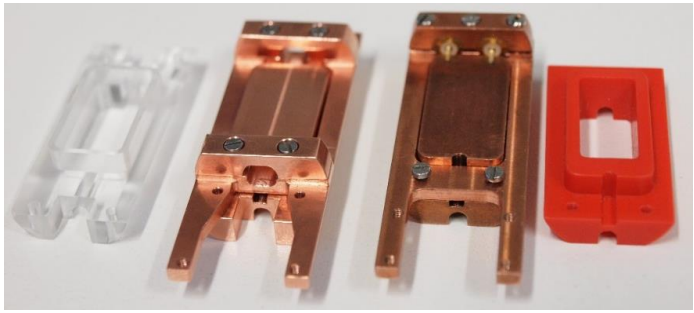

Figure 16: Microwave custom-made sample holders design. There are two different configuration for the straight and U-shape lines as well as two variations of the groundplane (conductive, dielectic).

The samples used for the deposition of organic monolayers can have different geometry. However, the 10x10mm or 10x20mm size samples are preferable, the wafer-size samples can also be used (Figure 17).

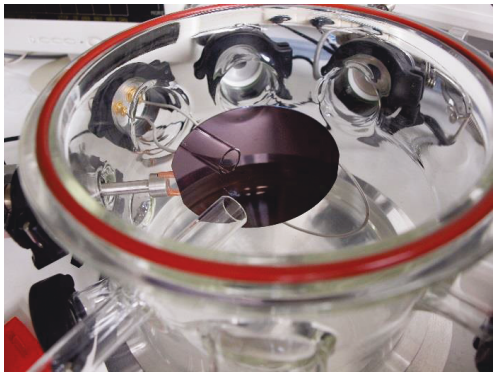

Figure 17: Wafer-scale deposition of self-assembling organic monolayers possible in GLOBUS device.

The oxygen plasma generator of this device is based on a modified conventional microwave oven, which generates a continuous RF-discharge with 700W power. The duration of the oxygen treatment is limited by the temperature rise inside the chamber (Figure 18a), which depends on the coupling of the microwave to the metallic sample holders in the chamber.

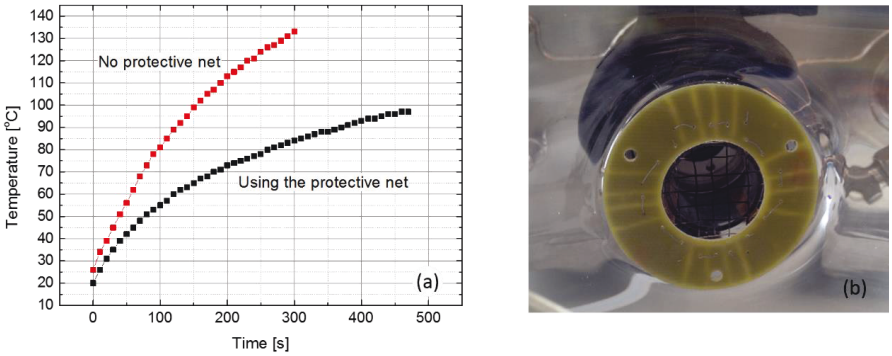

Figure 18: (a) Temperature rise inside the chamber with and without using the (b) protective net.

In order to reduce the coupling and to decrease the temperature rise inside the recipient, the metallic net is inserted (Figure 18b), which prevents the microwave radiation from entering the chamber.

Finally, for the in-situ electrical characterization, among others, a Network Analyzer (Hewlett Packard, 50MHz-20GHz) and a LCR-meter (Sourcetronic, 20Hz-2MHz) are used.

III.3.2 Deposition of organic molecular layers using GLOBUS device

The deposition of organic molecules typically works as follows. The cleaned sample is placed inside the sample holder and, optionally, reference samples are mounted in the microwave and capacitive sample holder respectively. The chamber is evacuated and purged several times in order to remove any contaminant gas. Then the chamber is filled with pure oxygen gas (99.9%) up to a pressure of about 1.4mbar. After that the RF-discharge is applied for 3 minutes to the oxygen flow inside the microwave oven and activated oxygen is generated. The activated gas is guided through the glass tube onto the substrate. Due to the activated oxygen organic residues are removed from the sample and the surface is activated which is implied especially for silanization process. Then the deposition process starts. The pressure in the chamber has to be set regarding to the evaporating pressure of chosen molecules. The beaker with molecules is connected to the chamber and the valve connecting the source of molecules with the recipient is opened. Molecules evaporate, follow the gas flow, enter the chamber and some of them deposit onto the substrate. Constant pumping partially removes the excess of molecular species. All in-situ characterization techniques register any small change of the electronic properties of the sample. They are mainly used to indicate start and termination of deposition of organic monolayers and to characterize properties of these monolayers during and after the deposition.

III.4 Preparation of graphene layers

For the deposition of graphene layers on different substrates, the cleanroom environment is necessary. In this work, we have used the graphene layers, deposited on different substrates by a "fishing" method. The preparation procedure is as follows:

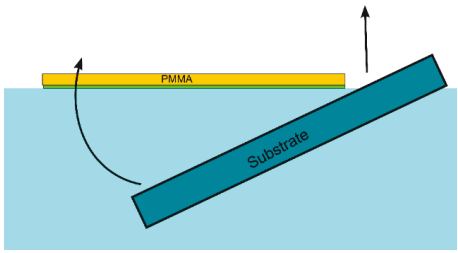

Figure 19: The "fishing" method of the deposition of graphene on different substrates.

1) Starting with Graphene/Cu foil, where the graphene is CVD-grown on both sides;
2) Spin-coating the PMMA on one side (approximately 400-500nm thickness) and anneal at 120-140°C;

3) O_2 plasma treatment of the back side to etch the backside graphene (300W, 200sccm, 15-20 sec);
4) Cutting if necessary;
5) Etching in ammonium persulfate $(NH_4)_2S_2O_8$ (0.1M solution) overnight;
6) Washing for 1 hour more in clean ammonium persulfate;
7) Rinsing in the DI water cascade;
8) Fishing the graphene out by a substrate as shown in figure 19;
9) Drying overnight;
10) Annealing at 150°C for at least 15 minutes;
11) Cleaning/etching the PMMA in acetone or hot acetone;
12) Rinsing in IPA (or chloroform);
13) Annealing in N_2 furnace at 300-350°C for at least 2 hours (with a slow ramp).

III.5 Preparation and functionalization of gold nanoparticles

Additional to relatively simple molecular layers, more complex systems have been investigated in this thesis. In bioelectronics, besides the chemical contrast, the surface topography can act as guiding cue for cell attachment [7], [8]. Even sub-100 nm structures are capable of influencing cells. For instance, gold nanoparticles (AuNPs), immobilized with defined interparticle spacing on surfaces, can serve as carriers of single peptide guidance factors [39]–[43] and functionalized with organic ligands [44], [45]. Furthermore, it has been recognized that, in particular, positively charged domains of peptides assist the adhesion of neurons[14], [46]. This finding was supported by the observation that positive charges associated with surface-bound, synthetic molecules containing amino groups can also promote the adhesion and growth of neurons [15]–[18].

Therefore, complex surfaces with AuNPs and molecular layers of different charges were prepared and characterized with an ex-situ analysis of the surface properties. The sample preparation is divided into several steps that are sketched in Figure 20 [46].

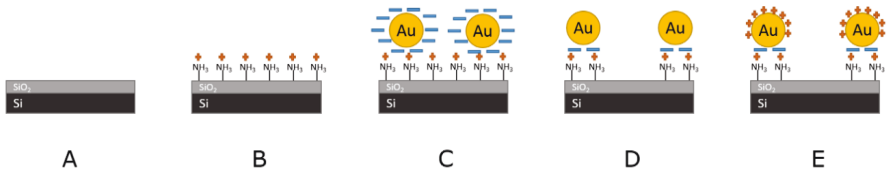

Figure 20: The schematic description of the process steps, i.e. A: Si and Si/SiO2 substrate, B: substrate functionalized with APTES, C: immobilization of citrate-stabilized AuNPs, D: removal of free citrates and APTES ligands, and E: decoration of AuNPs with aminothiols. For details, see text.

Step A: The samples are based on Si (100) substrates (n-doped) with a 100nm thick SiO_2 termination. The substrates are cleaned in clean room environment in several steps using the Protocol B. The quality of the Si/SiO_2 is controlled via ellipsometry (see Section III.6.1). This gives the reference point for further determination of the thickness of deposited molecular monolayer. Then, the samples are packed into the plastic container and transferred to the other building for the surface activation. Afterwards, the surface is activated using an oxygen plasma for 3 minutes at 200W power and 1,4mbar pressure in the oxygen plasma generator (Section III.2.2).

Step B: After the activation, the substrates are transferred to another laboratory, where they are functionalized with amino-terminated silane (3-aminopropyltriethoxysilane, APTES) leading to a positively charged surface (see Section III.2.4). The positively charged molecules are needed to create the electrostatic attraction of the negatively charged molecular citrate shell of gold nanoparticles. After one hour of the deposition, the samples are transferred back to the clean room building. Again, ellipsometry is used to control the properties and quality of the APTES layer. It provides an effective thickness of the silane layer, which converts to an effective coverage of the substrate with APTES, i.e. sub monolayer, monolayer or more than monolayer coverage can be distinguished. The typical thickness of the monolayer of APTES, according to [33] is in the range from 0.7 to 1nm. Furthermore, wetting angle measurements also provide indications for the coverage of the substrate with molecules (see Section III.6.2). The typical contact angle value for APTES molecules lies in the range from 45 to 60°.

Step C: After the quality of the molecular monolayer is proved by the ex-situ characterization via ellipsometry and wetting angle measurements, citrate-stabilized Au nanoparticles (AuNPs) are immobilized on the surface utilizing the electrostatic interaction between the negatively charged citrate shell and the amino-groups of silanes. In the chemical laboratory, in the other building, the samples are cleaned with the MilliQ water in order to remove not chemically bound molecules from the silanization process. Then all samples are dried and placed into the clean beaker. The conventional solution of nanoparticles (Sigma Aldrich), usually 20nm in diameter, is used. Exactly 111µl of the solution is dropped on each sample surface and left for at least 1 hour. After the time lapse, the samples are rinsed with MilliQ water. This concludes the immobilization process. At this step, the optical characterization via SEM was used to control the density of the particles deposited on the surface.

Step D: The free citrate ligands and APTES ligands are removed by oxygen plasma (2 minutes etching at previously mentioned conditions), leaving the bare AuNPs immobilized on the surface. After this procedure, the optical characterization via SEM is again used to control the etching process.

Step E: Finally, the AuNPs are decorated with various molecular monolayers (e.g. amino-1-undecanethiol) in order to obtain a positively or negatively charged surface that could, for instance, be used as an attractive interface for (guided) growth of neurons. The functionalization process is as follows. The conventionally prepared

molecules are solved in the solvent (typically ethanol) down to 0.05 or 1mM concentration. Then the samples with previously immobilized, etched and activated nanoparticles are placed into the clean and specially used beaker, where they are covered with 1.5ml of the prepared solution of molecules. The functionalization usually lasts about 18 hours. At the end of the functionalization, samples have to be cleaned with ethanol and MilliQ water in order to remove the residues. The optical characterization via SEM is finally applied after the immobilization procedure.

III.6 Ex-situ characterization methods

Next to the in-situ analysis via resistive, microwave and capacitive spectroscopy or surface acoustic wave measurements (see Section III.3), ex-situ characterization of the films surface is of importance. Some of these methods are presented in this section. The ellipsometry (see Section III.6.1) and water contact angle measurements (see Section III.6.2) are the most widely used techniques for the characterization of the quality of molecular layers on the surface because of their straightforward and reliable analysis. The streaming potential technique (see Section III.6.3) is used for analysis of interfaces formed by systems of different complexity and the electrolyte solutions. This analysis is very important for observation of the behavior of given systems in the biocompatible conditions in aqueous environment.

III.6.1 Ellipsometry

Ellipsometry is a very sensitive optical method for determining optical properties of a material. When an electromagnetic wave is incident on a medium, only part of it is transmitted into the medium. The fraction that is reflected depends on the complex refractive index, the angle of incidence, and the polarization state of the wave. For layers with different complex refractive indices, the fraction also depends on the layer thicknesses.

The two basic types of polarization are parallel, p, and perpendicular, s, polarization. The orientation of the electric vector refers to the plane of incidence, which is defined by the directions of the incident and reflected waves. The intensity-independent ratios of the amplitudes and phases of the reflected and incident p- and s-polarized electric fields are described by the complex reflectances r_p and r_s, respectively.

The complex reflectance ratio, ρ, of the system which is then given by the ratio between r_p and r_s:

$$\rho = \frac{r_p}{r_s} = \tan(\Psi)e^{i\Delta}, \tag{21}$$

where $\tan(\Psi)$ is the amplitude ratio upon reflection, and Δ is the phase shift.

Since ellipsometry is measuring the ratio (or difference) of two values (rather than the absolute value of either), it is very robust, accurate, and reproducible. Schematically, the ellipsometry principle is shown in the figure below:

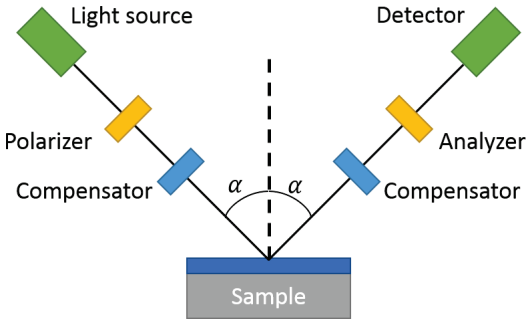

Figure 21: Ellipsometry measurement principle. The laser light beam is polarized by a polarizer and hits the surface. After reflection from the sample surface, the beam follows through the analyzer into the detector.

Ellipsometry is an indirect method, i.e. in general the measured Ψ and Δ cannot be converted directly into the optical constants of the sample. Normally, a model analysis must be performed. Direct inversion of Ψ and Δ is only possible in very simple cases of isotropic, homogeneous and infinitely thick films. In all other cases a layer model is needed, which considers the optical constants (refractive index or dielectric function tensor) and thickness parameters of all individual layers of the sample including the correct layer sequence. Using an iterative procedure (least-squares minimization) unknown optical constants and/or thickness parameters are varied, and Ψ and Δ values are calculated using the Fresnel equations. The calculated Ψ and Δ values, which match the experimental data best, provide the optical constants and thickness parameters of the sample.

III.6.2 Contact angle measurements

The contact angle Θ is the angle, defined by the liquid-vapor interface of a liquid on a solid surface (Figure 22). It quantifies the wettability of a solid surface defined by the thermodynamic equilibrium of a given system consisting of solid, liquid, and vapor. As

such the equilibrium contact angle reflects the relative strength of the liquid, solid, and vapor molecular interaction at a given temperature and pressure. Thus, the shape of a liquid drop on the surface is effected by the surface free energy and is therefore suitable for measuring surface properties.

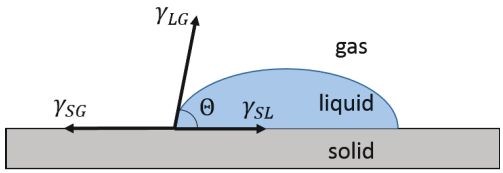

Figure 22: Contact angle Θ of three-phase solid/liquid/gas system with interfacial energies γ_{SL}, γ_{SG}, γ_{LG} of solid/liquid, solid/gas and liquid/gas interfaces respectively.

If the solid-vapor interfacial energy is denoted γ_{SG}, the solid-liquid interfacial energy is γ_{SL} and the liquid-vapor interface energy is γ_{LG}, respectively and assuming the perfectly planar surface the equilibrium contact angle can be calculated using Young equation:

$$\cos\Theta = \frac{\gamma_{SG} - \gamma_{SL}}{\gamma_{LG}} \tag{22}$$

A water drop spreads completely (absolute wetting case) on extreme hydrophilic surfaces. Large water contact angles ($\Theta > 90°$) indicate a hydrophobic surface. The contact angle is also the characteristic for the SAMs. For example, for the APTES monolayer, the water contact angle depends on the monolayer coverage. For a monolayer, the water contact angle at room temperature and atmospheric pressure is about 45-60°. For another type of molecules, 1H,1H,2H,2H-perfluorooctyltrichlorosilan (FOTCS), the typical contact angle is about 100°.

In our case the contact angle is determined via the sessile drop method. It is based on the investigation of the complete shape of a liquid drop lying on a planar solid surface. The image of the drop is captured with a camera and the contact angle is automatically recognized.

III.6.3 Streaming potential/current method

As discussed in Section II.3, the streaming potential/current method represents one of the four major electrokinetic methods used for the study of the so-called ζ potential, the electric potential at the plane of shear that is related to the surface properties but cannot be determined directly. The streaming potential technique is best suitable for investigation of planar samples, especially in bio-liquid environment, and therefore the best choice for the analysis of bioelectronic surfaces.

III.6.3.1 Electrolytes

By definition, an electrolyte is a substance that ionizes when dissolved in suitable ionizing solvent such as water. In this work, different electrolytes are used, which can be divided in two groups: working electrolytes and titration electrolytes.

As working electrolyte in most experiments the potassium chloride (KCl) in different concentrations (1 to 100mM) dissolved in the double distilled water (Bidest) is used, since it is a relatively simple and predictable system. Another working electrolyte is HBSS (Hank's Balanced Salt Solution), which is typically used for experiments with cells. HBSS consists of NaCl (8.4g), KCl (0.224g), HEPES (2.38g) dissolved in MilliQ water (1l). HEPES is a buffering agent with the chemical formula is $C_8H_{18}N_2O_4S$. The HBSS was chosen in order to examine interfaces of the initial environment of the cell growth. However, HBSS turned out to be too concentrated and not suitable for the streaming potential/current measurements in its original form. The diluted version of HBSS electrolyte was approximated with the simple KCl electrolyte, because it was assumed, that at low concentrations they have the same behavior.

As titration electrolyte for the acidic titration, mainly hydrochloric acid (HCl) in different concentrations (10-50mM) is used. For the basic titration, mostly the potassium hydroxide (KOH) in different concentrations (10-50mM) is used. Other titration electrolytes (e.g. H_2SO_4 (50mM) for the acidic and NaOH(50mM) for the basic titration) were used, but the advantage of the choice of KOH and HCl is that in combination they produce a salt, which will dissolve again:

$$HCl + KOH \leftrightarrow KCl + H_2O \tag{23}$$

III.6.3.2 Principle of the measurement

The current in the streaming current experiment is the result of the convective flux of ions arising from the thin double layer region adjacent to solid/electrolyte interfaces and conveyed by the flow of the electrolyte. The macroscopic flow of the fluid is usually provoked by the hydrostatic pressure gradient over the measurement cell. Due to charge separation caused by the flow, an electrostatic potential difference (streaming potential) appears along the interface, which is proportional to the streaming current. Thus, the determination of the ζ potential is based on a measurement of either the streaming potential or the streaming current. The magnitude and sign of the zeta potential provides conclusions on (a) the chemical, physical or molecular structure of

the surface, (b) the composition of the electrolyte solution and (c) the interaction between the solid and the liquid.

The streaming current/potential measurements are performed using a modified 'SurPass Electrokinetic Analyzer' (Anton Paar GmbH). The set-up is shown in Figure 23:

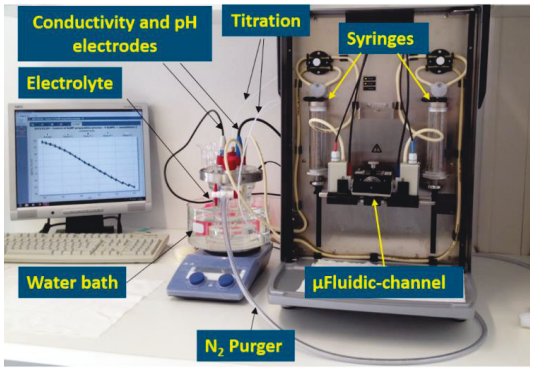

Figure 23: The overview of the streaming current/streaming potential set-up (electrokinetic analyzer (SurPASS)).

For measurement, a pair of identical samples (10x10 or 10x20mm size) is attached to the sample holders using the double-sided adhesive tape (Figure 24a,b). These two sample holders are mounted inside the holder (Figure 24c) to form a microfluidic channel. The distance between the coplanar surfaces is adjusted to form a channel with minimum width for a laminar flow of the electrolyte. The optimum width turned out to be between 90 and 150µm. This regime defined by technical requirements of the device and physical properties of the microfluidic channel. If the channel height is smaller than 90µm, a large pressure is needed to generate the flow, which can damage the syringes and influence the geometry of the channel. However, if the height of the channel is larger than 150µm in order to achieve good resolution, the flow rate will overcome the critical value of 600ml/min, which corresponds to the laminar to turbulent flow transition in this geometry. Therefore, it is recommended to adjust the height of the microfluidic channel to approximately 100µm.

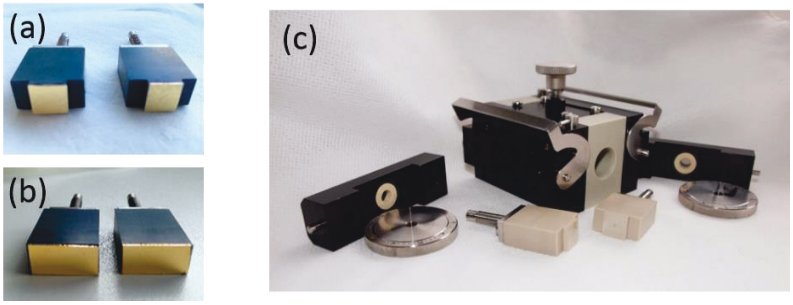

Figure 24: The samples are attached to the sample holder (a) or (b) and then placed into the holder (c) forming the microfluidic channel.

Next to the device is the reservoir with the working electrolyte solution (Figure 23). The properties of the electrolyte solution are controlled via temperature sensor, the conductivity sensor and pH electrode, which simultaneously measure the temperature in the range of 20 to 30°C, the conductivity in the range of 0.005-1000 mS/m and the pH in the range of 2-12pH, respectively.

The measurement setup was modified in order to get the reproducible and reliable measurements. In [47], we have already introduced the first modification, which was the water bath around the beaker with working electrolyte. This allowed the stabilization of the temperature of the electrolyte solution, which at the same time effects the stability of the ζ potential measurement, as it is recalculated using table values of viscosity, permittivity and cell constant, which are dependent on the temperature.

The second and the most important modification was the nitrogen purger, which is at the same time the beaker for the electrolyte, shown in Figure 23&Figure 25.

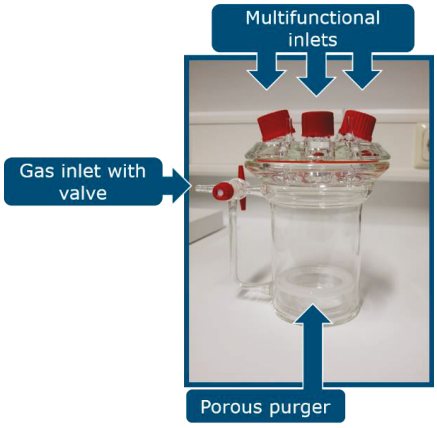

Figure 25: The nitrogen purger: a) the first and b) the latest concept.

The necessity of the purging the electrolyte solution arises from the dissolution of the CO_2 in water that is the solvent in all electrolytes we use. The solution rate of the CO_2 in water is around 750cm^3/l at 25°C. The dissolved CO_2 results in formation of charged ionic species additional to the electrolyte, considered as impurity, because they lead to the unpredictable behavior [48]:

$$CO_2 + H_2O \leftrightarrow H_2CO_3;\ H_2CO_3 + H_2O \leftrightarrow HCO_3^- + H_3O^+ \quad (24)$$

The solution of CO_2 has the overall negative effect, because it also leads to the change of the pH of the solution. In order to remove the CO_2, the inert gas has to be used. The argon and nitrogen both are good candidates for this. The nitrogen was chosen because of its availability and relatively lower price. The solution rate of the nitrogen in water is about 13cm^3/l at 25°C, which proves its indifference. Due to simple colloidal effects, the system tries to increase the entropy and save the energy, it is more preferable for CO_2 to come to the nitrogen/water interface and to be taken off from the solution. When purging with nitrogen, the pH of the solution has to correspond to the pure double distilled water pH value.

The preparation procedure is as follows. Samples are mounted with double-sided adhesive tape to the sample holders, which are mounted inside the holder, which is connected to the housing with the plug from each side. Each plug contains the pressure sensor and the Ag/AgCl electrode to measure the voltage or current, depending on the electrical circuit. The empty and dry glass beaker with a magnetic stir bar and with the nitrogen purger is prepared. The beaker is filled with the fresh prepared working electrolyte (typically, KCl, 1mM concentration). First, the system has to be rinsed with the working electrolyte. In order to avoid contaminations in the electrolyte beaker, the outlet hose is disconnected from the beaker cover and placed into a second glass beaker, which is used as the "waste beaker". The system is filled with 100ml of working electrolyte and afterwards, the electrolyte is poured out to the "waste beaker". Then the outlet hose is again plugged to the beaker cover and the system is now rinsed for 500s with the working electrolyte to establish the equilibrium. The height of the measurement cell is now adjusted and after the rinsing, the *flow check* procedure is performed to make sure that the system is filled without air and to check the parallel mounting of samples. In the case if, the samples are negatively charged at the neutral pH values, the acidic pH titration is necessary to achieve the isoelectric point. Therefore, the acidic titration electrolyte (e.g. HCl, 50mM) has to be prepared. In other case, the basic titration is required and therefore the basic titration electrolyte (e.g. KOH, 50mM) is used.

The measurement procedure is as follows. The pressure gradient is generated via the pair of motorized syringes that move synchronically, pushing the electrolyte through the measurement cell. There are different variations of the measurement cell for different sample geometries available from the company. The movement of a liquid through the capillary system creates a streaming potential or streaming current, which, together with the pressure, are registered by electrodes and pressure sensors, respectively. This data is then processed by the software (Visiolab by Anton Paar GmbH) and is shown as in the Figure 26:

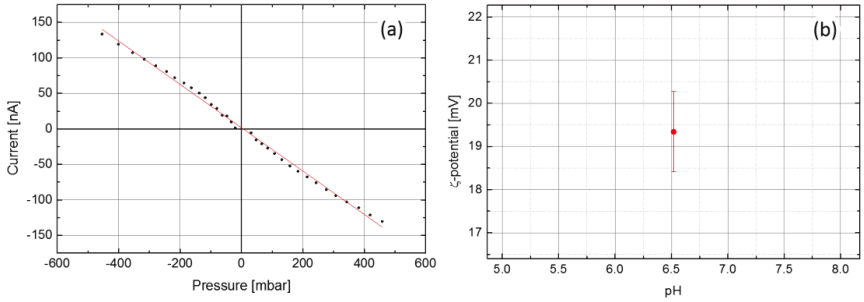

Figure 26: The measurement of the a) streaming current, recalculated to b) the ζ potential.

The streaming potential or streaming current vs pressure dependence (e.g. Figure 26a) is approximated with the line. The slope of this line is used to determine the ζ potential, which is given by [49]:

$$\zeta = \frac{dU}{dp} \times \frac{\eta}{\varepsilon \times \varepsilon_0} \times \frac{L}{A \times R} \tag{25}$$

and

$$\zeta = \frac{dI}{dp} \times \frac{\eta}{\varepsilon \times \varepsilon_0} \times \frac{L}{A} \tag{26}$$

where

ζ stands for zeta potential, $\frac{dU}{dp}$ – slope of the streaming potential versus pressure, $\frac{dI}{dp}$ - slope of the streaming current versus pressure, η - electrolyte viscosity, ε_0 - vacuum permittivity, ε – dielectric constant of electrolyte, L – length of the streaming channel, A – cross-section of the streaming channel, R – Ohm resistance inside the measuring cell.

Using relations (25) & (26) we obtain the values for the ζ potential at the given pH value (Figure 26b). If now, we add the titration electrolyte into the working electrolyte solution, the initial pH value (usually 5.5 to 7) is changed. Measuring the ζ potential (using the recalculation of the streaming current) at each pH value (Figure 27a), reached during titration, we obtain the pH dependence of the ζ potential, which is the main characteristic dependence for the samples that we examine. The example of such dependence, obtained using the pH titration of the initial KCl solution (pH 6.5) with the KOH electrolyte (up to pH 9) is shown in Figure 27b:

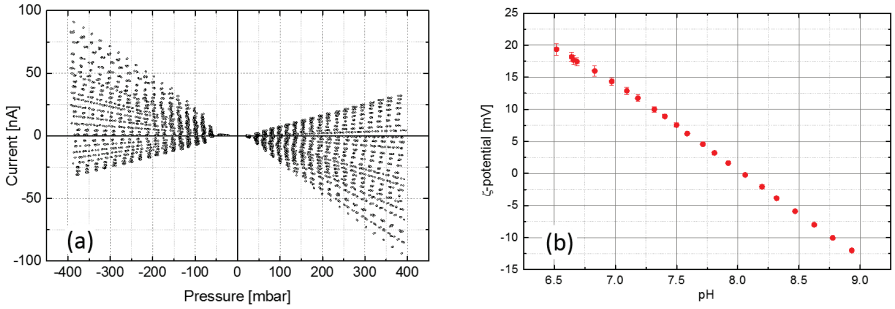

Figure 27: a) The streaming current vs pressure dependence at different pH values, recalculated to b) the ζ potential vs pH dependence, which is the characteristic of the examined sample.

The streaming current/potential technique is often used for determination of an important surface characteristic value - the isoelectric point. According to Section II.1.4, the isoelectric point corresponds to pH value where the ζ potential turns to zero.

Practically it means that in the case of the absence of specific adsorption we obtain the pH value at which the surface charge is completely compensated by the diffuse layer charge and equals to zero $\sigma^0 = -\sigma^d = 0$, which can supply us with the information on the surface composition. However, in the presence of the specific adsorption the isoelectric point moves from its original value. Specifically adsorbed anions will change the IEP to lower and cations – to higher values. The isoelectric point can be the indicator not only for the electrical properties of the surface, but also for hydrophilicity/hydrophobicity, the quality of the surface, degree of surface coverage, adhesive strength and effective chemical properties [50].

Nevertheless, the measurement is automated to some extent and performed using the conventional electrokinetic analyzer, it is still a challenge to obtain reliable and reproducible results because of many factors ranging from the proper cleaning of samples to the using of ultrapure electrolytes under special conditions and special measurement procedures. This forced us to introduce some modifications to the measurement set-up and measurement procedure, discussed in the following chapter.

IV. Results and Discussion

In this chapter, the modification and characterization of different surfaces are discussed, starting with simple interfaces (e.g. inert dielectric surface in contact with the aqueous electrolytes) continuing with more complicated systems (e.g. self-assembling monolayers of organic molecules and conducting noble metals), and ending with complex surface modifications (e.g. functionalized nanoparticles) especially for potential bioelectronic applications. In the beginning of the chapter, the optimization of the streaming current/streaming potential device and measurement procedure is shortly given, which was essential to obtain reliable results for the different systems that are examined.

IV.1 Streaming potential/streaming current reference measurements

In the first part of this section, the optimization of the measurement is sketched. Not all actions that have been taken are described. The discussion is restricted to the impact of the solvent (water) quality and optimization of the measuring procedure, using measurements on a perfect inert system, polypropylene foil, as a reference. Additionally, the hardly-avoidable impact of carbon dioxide, solved in the electrolyte, on the surface potential is analyzed and strategies to minimize this impact are developed.

IV.1.1 Optimization of the measurement procedure

In order to optimize the surface potential experiment, calibrate and verify the full functionality of the streaming current/streaming potential setup, validation measurements using polypropylene foil (PP foil) as a test sample are performed. Polypropylene is an isotactic polymer, which can withstand chemicals that are normally used during the measurement. This also means that the surface of the material is inert and has no net charge. Furthermore, it is hydrophobic and turns out to give very reproducible results that allow an accurate calibration.

Generally, surface charges at the interface between a hydrophobic solid and an aqueous solution are generated by (i) acid-base reactions of surface functional groups and (ii) adsorption of water ions (OH^- or H_3O^+). In case of the absence of surface functional groups (inert surface), only the second mechanism (adsorption of water ions) applies. This leads to a linear dependence of the ζ potential on the pH value and to an isoelectric point (IEP) value of 4, at which an equilibrium surface concentration of adsorbed

negative water ions (OH^-) and positive water ions (H_3O^+) is obtained [51]. Therefore, in titration measurements PP foil should demonstrate a linear dependence of the ζ potential on the pH value (behavior of inert surfaces) with an IEP of 4.0±0.2. [52]. Deviation from this behavior indicates that there are problems with the setup (e.g. impurities in the system) or with the measurement itself.

The surface potential is affected by many factors. In order to obtain reliable data, various factors are analyzed systematically, starting with different types of the solvent (water) for the electrolytes. Distilled, double distilled (BiDest) and MilliQ water are tested as a single electrolyte. Results, obtained for these measurements are shown in Figure 28:

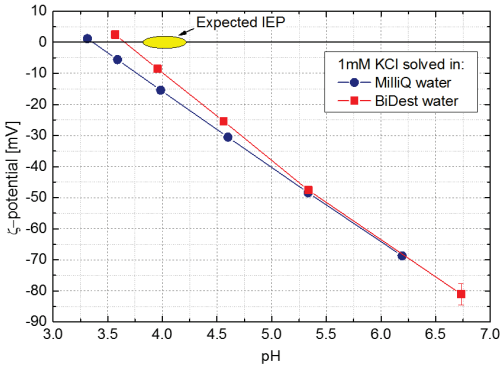

Figure 28: pH dependence of the ζ-potential of polypropylene foil measured with 1mM KCl solved in MilliQ (blue circles) and double distilled water (BiDest) (red rectangles).

None of the measurements yields an IEP of ~4, instead IEPs of 3.35 and 3.65 are obtained for MilliQ and for Bidest water, respectively. However, in all reference measurements the IEP of the measurement using Bidest was closer to the desired IEP, which indicates that the usage of the deionized water is preferable.

In the next step, potential contaminants of the electrolyte during the measurement are considered. Here especially the impact of CO_2 that forms carbonates and then might modify the surface have to be taken into account. For this, a N_2 purger (see Section III.6.3.2) that should reduce the amount of carbon in the electrolyte is developed. However, due to the safety reasons, the titration electrolyte is not purged with nitrogen, which causes CO_2 to enter the solution during titration. This means that the purger needs time to remove the dissolved CO_2 that gets into the working electrolyte with the titration electrolyte. This effect can be avoided by introducing additional rinsing and measuring steps after each titration step. This improved measurement procedure (using BiDest, N_2 purger and sufficiently long and repeated purging time to remove carbonates from the electrolyte) allows us to reproducibly obtain correct IEP values (red circles in Figure 29).

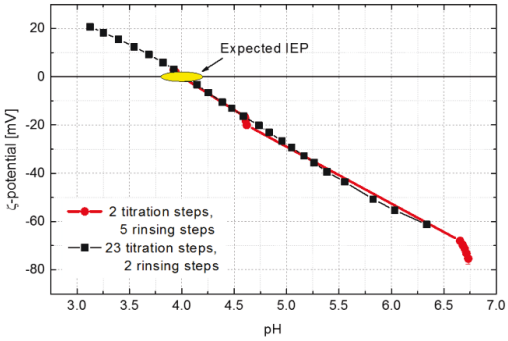

Figure 29: ζ potential as a function of pH of a PP foil for improved measurement procedures using BiDest water, N_2 purger and sufficiently long rinsing pauses in between titration steps.

In Figure 29 the pH dependence of the ζ potential with only 2 titration steps and 5 rinsing steps is shown in red circles. One can nicely see how the ζ potential develops (increases) with the additional N_2 purging. In order to have more precise experimental data, more experimental points are needed at different pH values. For this reason, the measurement procedure with additional purging and rinsing was optimized with respect to measuring and purging time. The black circles in Figure 29 show the pH dependence of the ζ potential with sufficient number of titration steps, including additional 2 rinsing steps at each measurement step. This curve agrees with the red curve with less titration steps perfectly and displays an IEP of 4, as expected for PP foil.

The removal of CO_2 turned out to be of great importance for the titration, as shown in the following section.

IV.1.2 Impact of carbon dioxide on the ζ potential

The titration of the working electrolyte is the important tool to analyze the surface potential in streaming current/streaming potential measurements. Via titration, the isoelectric point (IEP), can be determined, which represents a characteristic value for the surfaces. However, not only the IEP provides important information, also the dependence of the ζ-potential on pH value is important [25], [53]. In this section, the impact of the carbon dioxide on the pH-dependence of the ζ potential is discussed in detail.

Most of the electrolytes used for streaming potential measurements are water-based salt solutions with a pH value of water. Normally, the pH value of a pure water has to be approximately 7, which corresponds to the equilibrium of H^+ and OH^- ions in the solution (at 25°C). However, usually this is not the case, since water absorbs gasses from the atmosphere. These gasses when dissolved in water influence the properties of

the aqueous solution. The important component of the atmosphere that has to be considered is carbon dioxide (CO_2) which in water leads to the formation of carboxylic acid (H_2CO_3), and subsequently to the formation of carbonates (HCO_3^-). This acid shifts the pH value of water to ~5.5. This phenomenon not only affects the pH of the solution. Hydrocarbonates can adsorb on the surface therefore modifying the measurement. This is demonstrated in the following, using a borosilicate glass (BSG) substrates (10x20mm), standard KCl working electrolyte (10mM concentration), but no purger.

When starting the titration at the initial pH of the electrolyte (i.e. pH 5.5 without N_2 purger), the BSG substrates exhibit the expected inert behavior, with an IEP of ~3.9. Separate acidic (HCl) as well as basic (KOH) titration works flawless (see Figure 30).

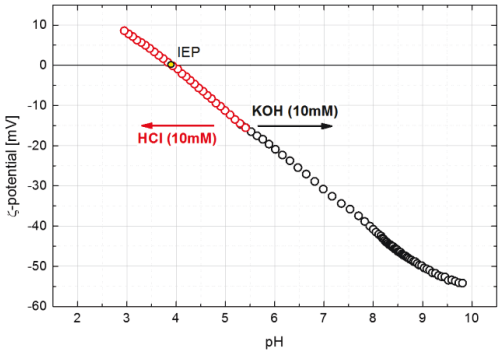

Figure 30: pH dependence of the ζ potential of borosilicate glass (BSG) substrates using separate acidic (using HCl) and basic (using KOH) titration.

However, interesting effects occur, if a basic titration is added after the acidic titration and vice versa. This is the usual procedure to measure the complete pH range in one run in order to analyze whether a surface is inert, basic, acidic or amphoteric.

Figure 31 shows two typical examples. In the first example (Figure 31a), 3.2ml of HCl (0.1M) are added to the initial working electrolyte solution of KCl (10mM) to obtain pH of 3. Then the working electrolyte is titrated with KOH (10mM) until pH of 10 is reached. As usual, other conditions (especially conductivity and temperature of the electrolyte) are controlled and kept constant. In the second example (Figure 31b), the starting point of the titration is pH of 5.5. Now, the working electrolyte is first titrated with the HCl to reach pH of 3 and then it is titrated back with the basic electrolyte (KOH) to pH of 9.

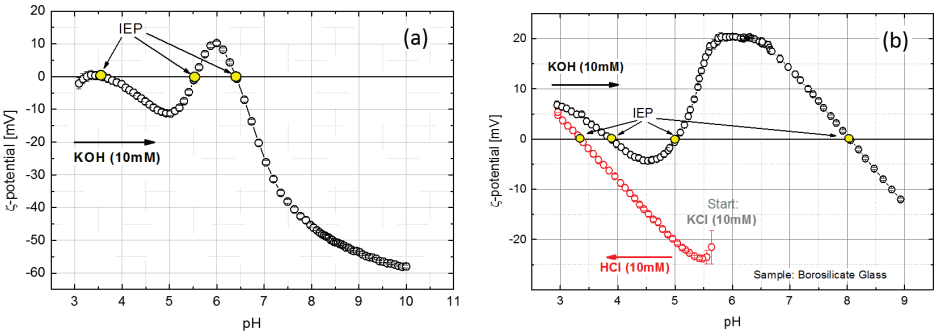

Figure 31: pH dependence of ζ potential of borosilicate glass for "complete" titration without N_2 purger. In both cases the experiment starts at pH of ~5.5 with an acidic titration using HCl (3.2ml HCl (0.1M) in one step (a) and HCl (10mM) in reasonable number of steps in (b)), followed by a stepwise basic titration using KOH (10mM).

The experimental data in Figure 31b shows that the first titration (acidic titration) of the BSG surface with HCl yields the typical behavior of inert surfaces with an IEP of 3.3 that correlates with literature data [54], [55]. However, the second titration leads to higher ζ potentials and an unusual peak in the pH dependence of the ζ potential around pH of 6. The shape of the curve for the second titration cannot be explained by inert, basic, acidic or amphoteric behavior, which leads to the conclusion that there is the chemical reaction, taking place at the surface.

However, we could demonstrate that the peak of the ζ potential at pH of ~6 is a result of CO_2 dissolved in water. Performing the same experiment as shown in Figure 31b on the same sample using the nitrogen purger, the pH dependence of the ζ potential for acidic and subsequent basic titration shows that the peak at pH6 is strongly suppressed (Figure 32).

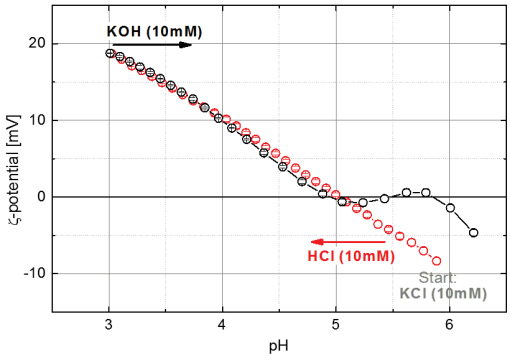

Figure 32: pH dependence of ζ potential of borosilicate glass for "complete" titration using N_2 purger. The experiment starts at pH of ~5.5 with an acidic titration using HCl (10mM), followed by a stepwise basic titration using KOH (10mM).

We conclude that the nitrogen replaces CO_2 in the electrolyte solution during purging and at the same time does not react at the surface. The small peak at pH of ~6 might be caused by remaining carboxylic acid from the titration agents, which are only purged after it is added to the working electrolyte.

Thus, the nitrogen purging is very important in our electrokinetic experiments, due to the dissolved CO_2, which strongly influences the properties of the electrolyte, surface, and consequently the correct measurement of the ζ potential.

IV.2 Simple interfaces: Dielectrics

In this section, the pH dependence of the ζ potential of 'simple' interfaces (typically planar, inert, polished, and chemically cleaned substrates) is discussed. As examples, the behavior and isoelectric points (IEPs) of borosilicate glass (BSG), different orientations of Si and r-cut sapphire are discussed. In the second part, Si (100) surfaces, modified with 100nm SiO_2 layer and treated with oxygen plasma are presented.

Si and BSG are maybe ones of the most suitable substrates for bioelectronics. BSG consists of silicon dioxide (>80%) with addition of boron oxide (>10%) and some other minor oxides. This content makes the BSG surface very similar to the silicon surface that possesses 3nm native oxide layer. In this work, silicon is represented by Si (111), Si (100) n-doped and, later in this section, SiO_2 oxidized Si (100). Sapphire (r-cut) represents the substrate, which is widely used in thin film deposition as well as in microwave circuits. In this work, it is mainly used as a reference surface to biocompatible Si and BSG.

For investigation of given surfaces, the standard measurement procedure, established in Section IV.1.1, is used for acidic titration using hydrochloric acid (HCl, 50mM) as titration electrolyte and potassium chloride (KCl, 1mM) as working electrolyte also including the N_2 purger. The acidic titration allows obtaining the IEPs for all samples that are negatively charged at neutral conditions. All samples are 10x10mm in size, chemically cleaned using Protocol A (see Section III.1).

The pH dependences of the ζ potential for BSG, a pair of Si and sapphire samples are shown in Figure 33 in comparison to the calibration curve, obtained by using the polypropylene foil.

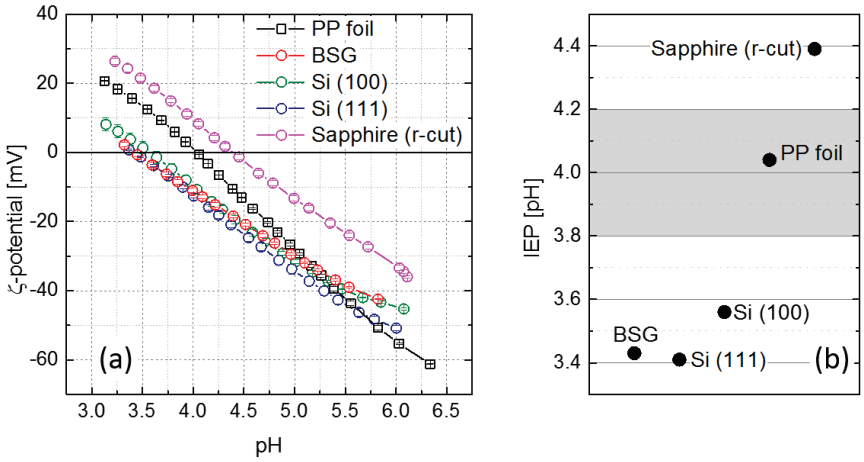

Figure 33: a) pH dependence of the ζ potential and b) isoelectric points of 'simple' dielectric interfaces (i.e. borosilicate glass, silicon (111) and (100) orientation, r-cut sapphire) in comparison to the polypropylene foil. The shaded region in (b) marks the regime of hydrophobic inert surfaces.

The pH dependence of the ζ potential of all samples demonstrates that all surfaces are inert (no basic or acidic groups dissociating from the surface) (Figure 33a). The main difference of investigated surfaces lies in the IEPs (Figure 33b). Starting with Si, interestingly, there is a small difference between the two different crystal orientations. The (111) orientation seems to be slightly more acidic (i.e. it possesses more negative charges on the surface). However, the difference is relatively small. As expected, the IEP of the BSG is very similar to that of the silicon surfaces. Actually, it seems to lie between the IEPs of the two orientations of Si. All surfaces are hydrophilic and the IEPs are in the good agreement with literature data for silicon and silicon oxide surfaces [54], [55].

The surface potential of r-cut sapphire is generally higher than that of the Si-based substrates. The IEP, determined for the r-cut sapphire surface is of 4.39, which is in agreement with literature. However, there are also studies with diverging IEP values for sapphire. The reason is the different surface structure dependent on the cut [56], [57], which can lead to positively charged surface even at neutral and physiological pH. For extended characterization of this kind of surface, one should also refer to [47].

In further experiments, Si (100) n-doped surfaces are investigated since it is a widely used substrate for bioelectronic experiments. Thus, n-doped and SiO_2 terminated substrates typically represent the starting point of all sample preparations. Although, the Si surfaces are well studied by different electrokinetic methods [55], [58]–[63] small differences depending on the termination or activation of the surface might be important. For this reason, we studied the difference between n-doped Si with a 3nm native oxide surface and with a 100nm SiO_2, obtained by thermal oxidation. Additionally,

the oxidized surface was activated using an oxygen plasma (see Section III.2.2.1). The resulting pH dependences of the ζ potential are given in Figure 34.

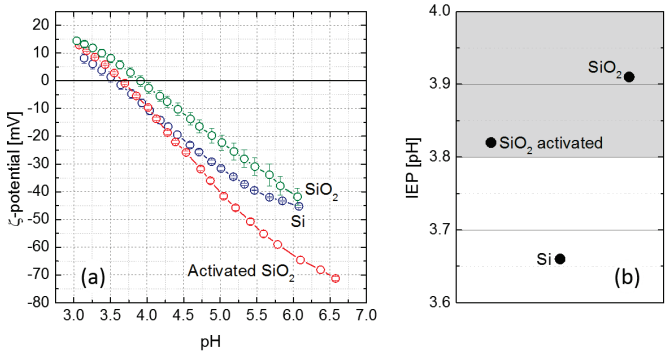

Figure 34: pH dependence of the ζ potential of n-doped Si (100) after cleaning (blule circles), with additional 100nm SiO_2 layer (green circles) and additional oxygen activation (red circles). The shaded region in (b) marks the regime of hydrophobic inert surfaces.

All samples show an inert behavior. The original Si surface possesses the smallest IEP of 3.56. The slight curvature at low pH values should not be considered. It is always present at low pH values due to the large density of counter-ions in the electrolyte and can be treated in terms of overcharging effects [29] which is also known for the silanol bonds [10]. The SiO_2 terminated surface tends to have a slightly higher ζ potential for the complete pH regime and therefore a slightly higher IEP of 3.91. This means that there is more positive charge on the surface (most likely specifically adsorbed hydrogen ions coming from electrolyte solution [64]) and therefore less additional positive charge is needed to reach the IEP.

Finally, the activation of the SiO_2 surface in an oxygen plasma leads to a cleaning and oxidation of the surface layer of silicon and therefore to increased number of silanol bonds. Later, they serve as bonding sites for silane molecules (e.g. FOTCS or APTES). In aqueous environment, the silanol bonds are protonated leading to hydroxyl surface functional groups that are highly negatively charged. Consequently, the ζ potential of the surface is strongly reduced with respect to the non-activated surface (-70mV compared to -40mV at pH of 6). One would expect that an increased number of silanol groups, which are acidic, would lead to an IEP in a very acidic region. However, this is not the case. Around pH of 5.5 the slope of the pH dependence changes and the IEP ends up to be similar to that of the non-activated surface. This is a clear indication of the reconstruction of silanol bridges, which was also reported in [36].

IV.3 Metallic surfaces

The measurement of the surface potential of films with a large surface conductance is difficult and only possible in streaming current measurement that excludes the influence of surface conduction. Generally, metallic surfaces (noble metals) are of interest for bioelectronic applications, since they are used as electrode materials as well as substrates for molecular monolayers (e.g. thiol bonding) facilitating cell adhesion. Another advantage of using noble metals is their resistance to oxidation and stability in physiological conditions. In this section, we will discuss the characterization of metallic films of Pt, Au and Cr deposited via thermal evaporation onto the borosilicate glass substrates (Figure 35) in the clean room class 100 environment.

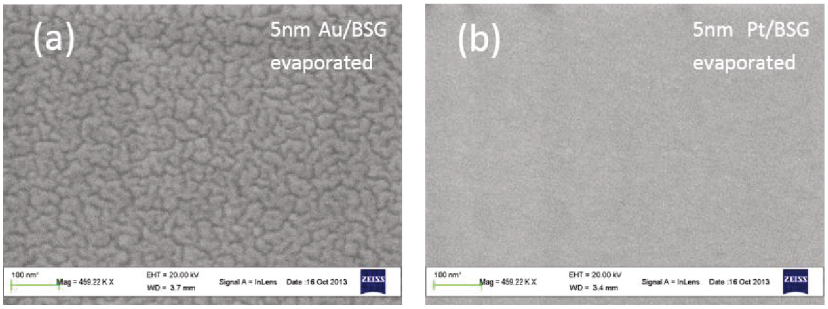

Figure 35: SEM images of noble Au (a) and Pt (b) thin (5nm) films evaporated on borosilicate glass substrates.

The toxic to organics metal Cr is chosen as the reference surface to noble and biocompatible Au and Pt surfaces. The pH dependence of the ζ-potential measurement (Figure 36) is done using our standard measurement procedure for 10x10 samples for negatively charged surfaces, i.e. acidic titration.

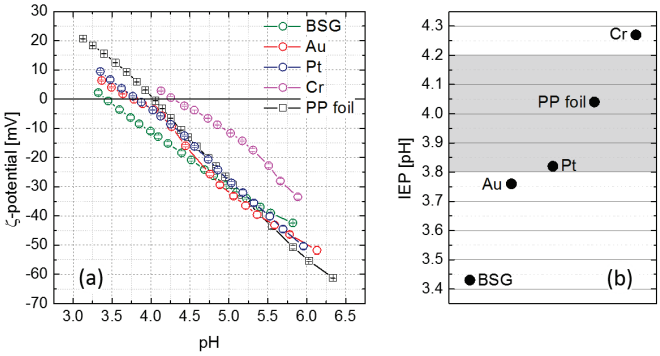

Figure 36: a) pH dependence of the ζ potential and b) isoelectric points of 5nm thick evaporated metallic films (Au, Pt and Cr) on BSG, the substrate (BSG), and inert polypropylene foil. The shaded region in (b) marks the regime of hydrophobic inert surfaces.

Figure 36 shows that the IEPs of all films are higher compared to that of the substrate. All metal surfaces when getting in contact with the aqueous solution can be divided into two groups:

(i) either they immediately form an oxide layer (hydrophilic)
(ii) or they are inert to water (hydrophobic).

When measuring metals from the first group, the electrokinetic properties of metal oxides are dominant. Cr belongs to this group. It forms a passivation oxide layer, when getting in contact with the electrolyte, which leads to a relatively positively charged, but still hydrophilic surface. The measured IEP of Cr is of 4.27, which agrees with the literature [65]. Typical IEPs of other metals from this group can be found in [55], [61]. The second group interacts with ions in the solution via the so-called hydrophobic interaction, i.e. the negatively charged OH^- groups are specifically adsorbed on the surface. As a result an IEP of 4 is expected similar to that of the inert organic polymer compound polypropylene. The characterization of gold layers using streaming potential method was already performed by different investigators [66], [67]. They obtained IEPs ranging from 2.9 to 4.5. In our experiment (Figure 36) the Pt and Au layers show an IEP of ~ 3.8, which is slightly lower than expected (IEP of 4 is expected for optimized inert, hydrophobic surfaces), but still within the expected region. This result suggests that the surfaces of these films might not be perfectly clean, although they were evaporated in clean room environment. However, we will show below, that this is most likely not the case. It seems that these films are activated during the deposition.

In order to test the effect of chemical cleaning and plasma activation on metallic surfaces, Au film was specially cleaned using protocol A and activated using the oxygen plasma. Figure 37 nicely shows the 'history' of this series of treatments. It should be noted, that in this case acidic titration (first 2 data sets) and basic titration (last 2 data sets) have been applied. Starting with the original Au layer (as obtained after deposition and stored in a plastic container), a slight amphoteric behavior with a reduced IEP of 3.76 is observed. Chemical cleaning (protocol A) leads to the inert behavior and generally increases the ζ potential. In this case, an optimal IEP of 4 is achieved. Activation of the layer (oxygen plasma generator, 120W, 0.8mbar, 5min) leads to the expected strong reduction of the ζ potential. Finally, if we immerse the layer in ethanol (99.9%, 10min) after the activation, the ζ potential is increased again. It is back to the about the same level that was observed before the activation.

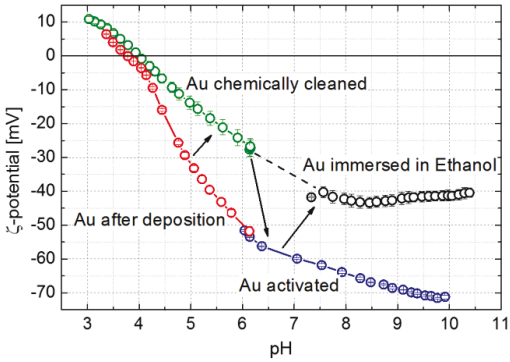

Figure 37: pH dependence of the ζ potential for a gold surface directly after the deposition (red), chemically cleaned (green), activated in oxygen plasma (blue) and immersed into the ethanol after activation (black). The dashed line serves as a guide for the eye. It connects the final step with the measurement before activation.

Interestingly, the pH dependence of the ζ potential of the Au surface activated in plasma is the exact extension of the pH dependence of the sample, measured directly after the preparation. This suggests that the Au surface undergoes some ion treatment (e.g. bombardment) or is annealed in oxygen atmosphere during deposition. Moreover, the behavior of the activated sample immersed in ethanol represents an extension of data for the chemically cleaned sample. This suggests that the immersion of the Au layer in ethanol eliminates the activation effect.

In conclusion, these results tell us that the treatment of the metallic layer play a very important role for the surface properties. Even a single monolayer of contaminant or an influence of a modification of the surface layer can significantly decrease or increase the surface potential.

IV.4 Graphene

Due to its unique properties (monolayer thickness, good conductance, mechanical and chemical stability), graphene represents one of the most interesting new potential alternatives for Si/SiO_2 in bioelectronic applications. However, graphene, being a thin monolayer, has to be supported by a substrate in any application. Therefore, the motivation for this set of experiment is to investigate

(i) the surface potential of graphene itself and
(ii) the potential influence of the substrate on the surface potential of graphene layers.

The information about the electrical surface properties of the substrate-graphene system in an aqueous solution might, for instance, be of great importance for FET

biosensor devices. The right choice of the substrate can influence the properties of the graphene layer and therefore the adhesion of the biomaterial and consequently the performance (i.e. selectivity and sensitivity) of the sensor of FET-based devices.

The graphene layers are deposited by the 'Finishing' method (see Section III.4) in the cleanroom environment. Figure 38 represents the pH dependence of the ζ potential for graphene on different types of substrates in comparison with the data obtained for the original substrates (after chemical cleaning) and substrates chemically cleaned and annealed in N_2 (350°C, 2 hours). The substrates have been chosen according to their potential applicability and IEP values of ~ 4 (Si/SiO_2, Kapton), <4 (BSG), and >4 (r-cut sapphire).

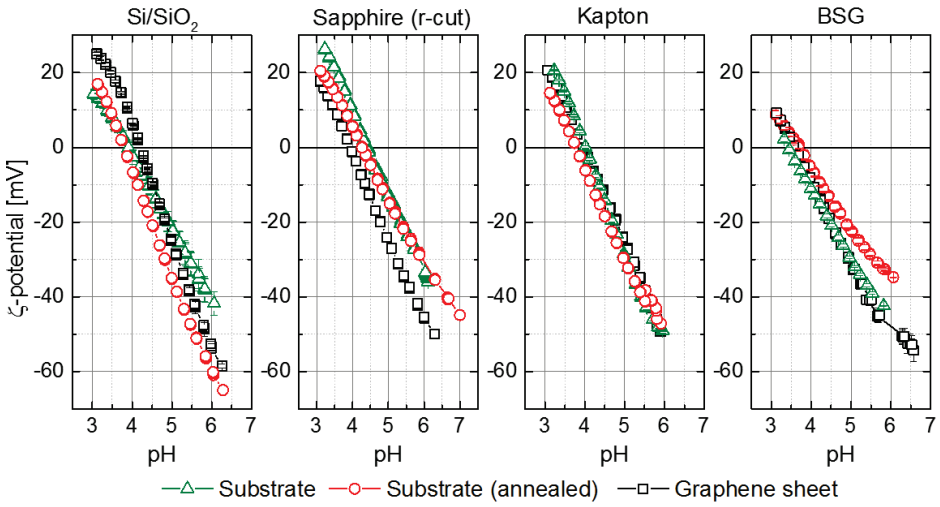

Figure 38: pH dependence of the ζ potential for graphene (black squares) deposited on different substrates. For comparison, the data for the cleaned (green triangles), and in N_2 annealed (red circles) substrates are shown.

The coverage of the substrates by graphene is nearly 100% for each substrate. The pH dependence of the ζ potential (Figure 38) indicates that the graphene layer is inert. It shows a linear behavior over a large pH regime and, moreover, it seems to be hydrophobic (see Figure 39), since the isoelectric point obtained for almost all samples lies in the "hydrophobic IEP region", defined by pH of 4±0.2.

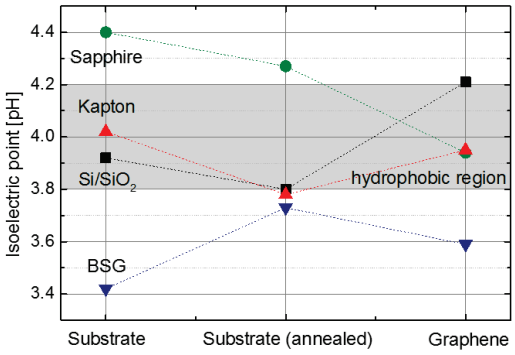

Figure 39: Comparison of IEPs for graphene layers on different substrates, original substrates and N_2 annealed substrates. Lines are guides for the eyes. The shaded regime represents the regime of IEP for hydrophobic materials.

The N_2 annealing of BSG, Si and Kapton seems to lead to very similar IEPs, whereas the IEP of the sapphire is different. However, the N_2 annealing influenced all surfaces. Generally, it can be noted, that the graphene layer does not lead to a significant modification for the hydrophobic surfaces Si/SiO_2 and Kapton. Therefore, we conclude, that the IEP of graphene itself is about pH of 4. This is supported by the result obtained for BSG and sapphire. In both cases the IEP of the graphene layer on these substrates is shifted in (sapphire) or towards (BSG) the hydrophobic IEP regime (see Figure 39).

IV.5 Molecular monolayers

In this section, the surface potential as well as in-situ (microwave and capacitive spectroscopy) and ex-situ (contact angle and ellipsometry) characterization of molecular layers deposited on BSG and Si are discussed. As example, two silanes are considered: 1H,1H,2H,2H-perfluorooctyltrichlorosilane (FOTCS) and 3-aminopropyltriethoxysilane (APTES), presented in Figure 40.

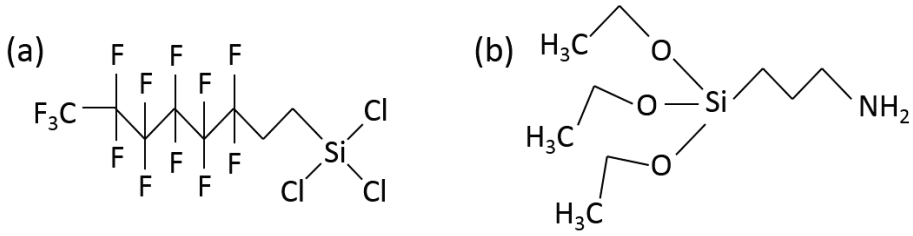

Figure 40: Chemical structure of (a) 1H,1H,2H,2H-perfluorooctyltrichlorosilane (FOTCS) and (b) 3-aminopropyltriethoxysilane (APTES).

The silanization procedure was done by vapor phase deposition (see Section III.2.4) that should produce high-quality self-assembled monolayers compared to the deposition from a solution.

In a first test, we deposited FOTCS to optimize and check the deposition of molecular layers in the new device (GLOBUS). FOTCS molecules solution (97%) is inserted into the transport beaker in a Glove Box under Ar atmosphere and then it is transported and connected to the silanization device (GLOBUS). By reducing the pressure to 45mbar, i.e. the evaporation pressure of these molecules, the deposition starts. The pressure of 45mbar is held for an hour, i.e. long enough for the deposition and formation of a monolayer of molecules.

The deposition is monitored in-situ via microwave and capacitive spectroscopy. Furthermore, ex-situ ellipsometry and contact angle measurements are performed to verify the deposition of the monolayer.

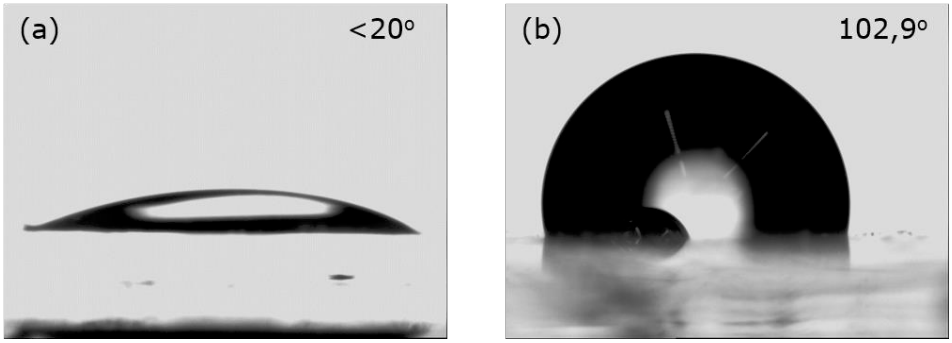

Figure 41: Contact angle measurements (a) before and (b) after silanization of a borosilicate glass with FOTCS in the GLOBUS device.

Before silanization, the cleaned and activated substrate (BSG) shows a complete wetting ($\Theta<20°$) that is indicative of the hydrophilicity due to open silanol bonds (see Figure 41). After silanization, the surface is hydrophobic, $\Theta\approx103°$. The surface properties are modified due to the deposition of FOTCS. The thickness of the layer is estimated via ellipsometry. Typically, the thickness of the monolayer of FOTCS is about 1-1.2nm.

Silanization with APTES is nowadays widely used in different scientific areas [10], [33]. This molecule is similar to FOTCS and therefore the silanization procedure is very similar. The pressure is carefully reduced and the evaporation of APTES sets in at a slightly lower pressure of 0.09mbar. It is visible in form of a small increase in pressure up to 0.22mbar. The silanization time is chosen similar, i.e. 1 hour. The deposition is monitored by microwave and capacitance spectroscopy. After deposition, the films are characterized ex-situ by contact angle measurements and ellipsometry.

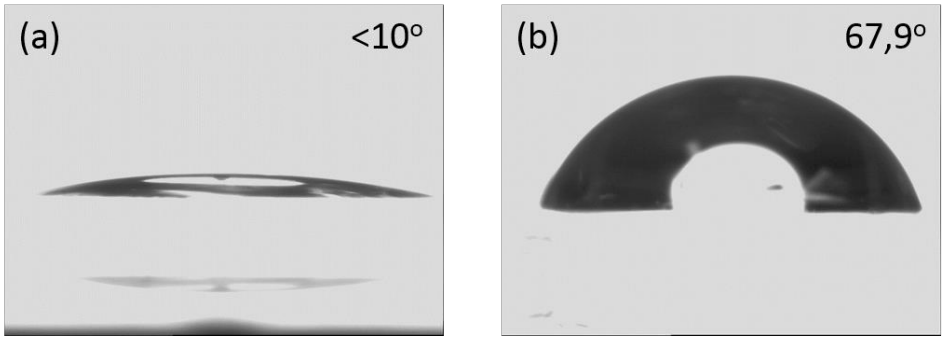

Figure 42: Contact angle measurements a) before and b) after the silanization of the borosilicate glass surface with APTES in the GLOBUS device.

The contact angle of the APTES terminated glass surfaces (Figure 42b) is close to the angular rate of 45-60° that is reported for APTES [38]. This is an indication of the slightly thicker layer (i.e. more than one monolayer). This result is in a good agreement with ellipsometry data that revealed a thickness of the molecular layer of 1nm, which is slightly larger than the literature value of 0.7±0.2nm for a monolayer of APTES.

The surface potential determination measurements of APTES are discussed in the following chapter.

IV.6 Complex interfaces: Functionalized gold nanoparticles and organic molecular monolayers

Gold nanoparticles (AuNPs) represent an extremely interesting tool that can, for instance, be used in bioelectronics since they can be functionalized with molecular monolayers, facilitate the protein adsorption and hence, affect and improve adhesion, growth and guiding of living cells on a surface. Moreover, they are macroscopic objects and therefore can easily be detected using the scanning electron microscopy (SEM), which allows the structuring and manipulation of their distribution on a surface [46]. A nice example of the guiding of neuronal cells via amino-functionalized AuNPs is presented in Figure 43.

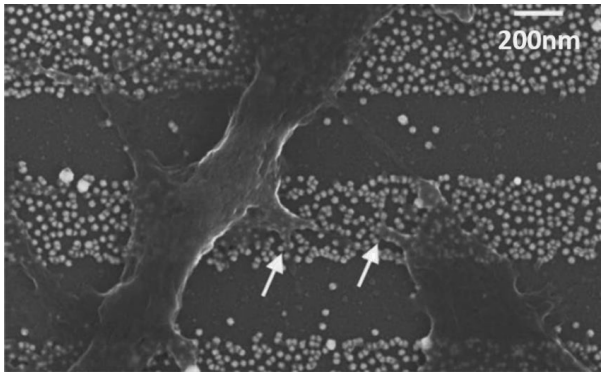

Figure 43: SEM images of neurons growing on amino-1-undecanethiol covered AuNP structures. Arrows indicate anchor points of neurites. Source: [46].

The surface potential of a complex surface for potential bioelectronic applications consisting of various compounds (i.e. bare substrates, organic molecules with different functional groups, and AuNPs) represents a very interesting and demanding object for our surface analysis via streaming potential/current technique.

In this section, a complete process of AuNPs immobilization and different functionalizations starting from the bare surface to AuNPs covered with molecular monolayers is discussed. It includes detailed analysis of APTES molecular monolayers, AuNPs immobilized on Si and BSG surfaces, and functionalization with varies molecular monolayers that possess different charges. Additionally, the effect of the concentration of AuNPs on the ζ potential of the interface is discussed.

In order to investigate the modification of the surface potential during the process of the immobilization and functionalization of AuNPs, detailed streaming current measurements are performed as function of pH and time for each part of the preparation process. Since for each preparation step a new set of samples is used, an additional control of different process steps is required, i.e. ellipsometry and wetting angle characterization are used to monitor the thickness and hydrophilicity of the initial APTES layer and electron microscopy (SEM) is used to analyze the AuNP distribution. In nearly all cases the ellipsometry revealed a thickness of the APTES layer of (0.7±0.2)nm and a wetting angle of (40±4)°. Both values agree reasonable well with the expected value for monolayers of APTES [33], [46].

The pH dependence of the ζ potential data is given in Figure 44a-e, representing different steps that are discussed separately.

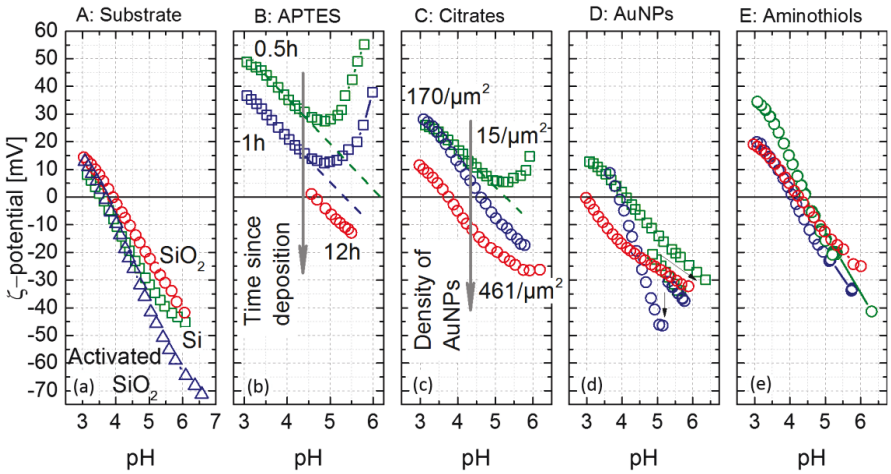

Figure 44: pH dependence of the ζ potential of: (a) bare substrates Si, Si/SiO_2 and oxygen activated Si/SiO_2, (b) after deposition of APTES (measured different time after APTES deposition), (c) after deposition of citrate-stabilized AuNPs (different AuNP concentrations are given), (d) after removal of free molecules (citrates and APTES) via oxygen plasma, and (e) after deposition of amino-1-undecanethiols onto the AuNPs. Each curve represents a different pair of samples, however, experiments in the same symbol (and color) belong to one series of measurements (e.g. identical density of AuNPs), and excluding step A, which is the same for all. Additional lines in (b) and (c) indicate the extrapolation of the measurement that is used to obtain an IEP value for some of the measurements.

Step A, pure substrate: The n-doped and SiO_2 terminated substrates represent the starting point of all sample preparations. These surfaces are typical representatives of 'relatively simple' interfaces, where only the solid surface and liquid electrolyte are brought into contact. The data and discussion of the substrate material was already given in Section IV.2 and is shown in Figure 44a for comparison with other measurements. However, here we additionally discuss the time dependent measurement at a fixed pH of 6 (Figure 45) that demonstrate that the ζ potential of non-activated SiO_2 terminated Si (black open circles) is unaltered over the complete measuring time of ~ 6h. However, the plasma-activated SiO_2 surface, as also reported elsewhere [60], [68], is unstable in time during dry or wet storage. In our particular case, the ζ potential of the activated SiO_2 surface is decreasing from -70 to -80mV during 4h and then remains stable. This effect is not yet completely understood, but is probably the result of the oxygen plasma treatment that increases the quantity of silanol groups on the surface, which are reconstructed in time.

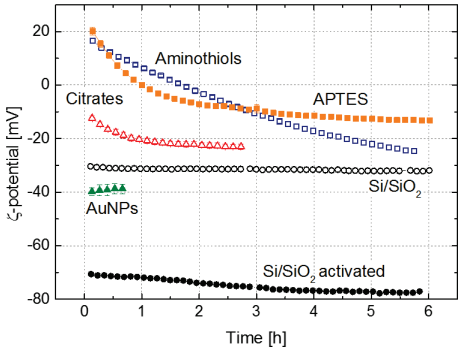

Figure 45: Time dependence of the ζ potential of Si/SiO_2 substrate (open circles), Si/SiO_2 substrate, treated by oxygen plasma (solid circles), positively charged layer of APTES molecules (solid squares), positively charged layer of amino-1-undecanethiols pinned on the AuNPs (open squares), citrate-stabilized AuNPs on APTES possessing both negative charges from citrate-molecules on gold and positive charges from APTES (open triangles), and plasma-treated bare AuNPs on a bare substrate (solid triangles). All measurements were executed at pH of 6.

In conclusion, the Si/SiO_2 surface of the substrate seems to be stable and inert until it is activated with oxygen plasma.

Step B, APTES: Figure 44b presents the pH dependence of the ζ potential of the silicon oxide surface after deposition of a monolayer of APTES molecules. The figure displays three sets of data that are recorded after different times that elapsed after the deposition of the molecular layer. The 'fresh' sample (only 0.5h after deposition, green squares) shows an unusual behavior. Starting at neutral pH values, the ζ potential is very high (around +60mV at pH of 6). Such high potentials are referred to as unstable in [25]. However, the APTES molecules are protonated in the aqueous solution and such a high potential is only an indication for high molecular density on the surface. With acidic titration, the ζ potential of an inert or 'standard' system is expected to increase due to the number of protons coming into the solution. However, the ζ potential of fresh $APTES/SiO_2$ system first decreases (until pH 4.8) and then starts increasing. The other sample, which was stored for a little bit longer time (1h, blue squares) before the measurement started, shows a similar behavior, however at a relatively lower level of the ζ potential. Interesting, that after a delay time of 12h an inert pH-dependence of the potential is observed (red circles). It starts with a negative ζ potential value and increases linearly with decreasing pH value. These observations are also supported by the time dependent measurement of the ζ potential (Figure 45&Figure 46) for APTES sample. Starting with the positively charged surface, the ζ potential decreases strongly with time and finally becomes low negative.

Such behavior, as also reported in [69], is assigned to the loss of the surface groups, and the initially positively charged surface becomes even negatively charged at a certain point. In our case, this process took 1.5-2h. Additionally, after 6h of measurement time,

the ζ potential of the surface is more or less stable, however, it is still positively charged compared to the bare substrate.

Thus, the starting point of the pH-dependent as well as time-dependent measurement depends on the time spent after the preparation. During this time, the deposited molecules that are not strongly bound to the surface are desorbed. This conclusion is also supported by the result, shown in Figure 46, where two samples were prepared using the same procedure, but one sample was left longer in the chamber in order to pump out the "rest" of the molecules.

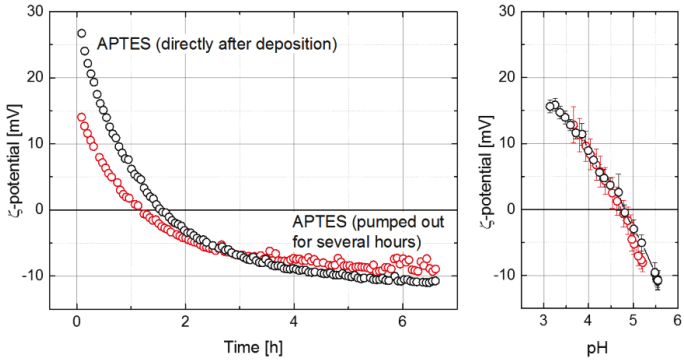

Figure 46: (a) Time dependence (measured at a pH of 6) and (b) pH dependence of the ζ potential of APTES monolayers on Si(100).

The starting points of both sets are different (15 vs 28mV), however, the saturation value is similar, -10mV. The starting point is higher for the surface that is taken out of deposition chamber directly after the deposition.

From this we conclude that molecules are desorbed from the surface during the storage as well as during the electrokinetic experiment. The desorption process persists for several hours (≈ 6h in our experiment) until a stable state is reached. The surface is still more positively charged relative to a bare substrate, which indicates that the remaining APTES molecules are sufficiently strongly bound.

The initial behavior of the pH dependence of the ζ potential of fresh prepared APTES layers (Figure 44b) is therefore a combination of

(i) the decrease of the ζ potential with time due to the desorption of APTES molecules and
(ii) an increase of the ζ potential due to the titration.

If we now assume that the impact of desorption on the ζ potential decreases strongly with time, we can estimate the IEP of the resulting APTES layer from extrapolation of the last part of the data that are taken at low pH values. The lines in Figure 44b indicate

the extrapolation. The resulting IEPs (Figure 47), therefore, decrease in time after deposition. In Figure 47 the extrapolated values of IEPs are shown with squares, whereas the measured IEP values are shown with circles.

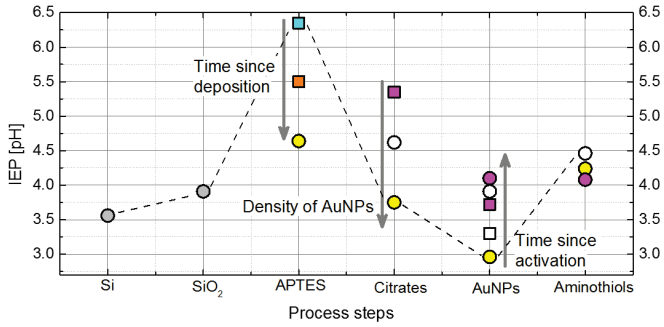

Figure 47: Resulting IEPs for the different process steps of immobilization and functionalization of gold nanoparticles, given in Figure 44. The dashed line shows the resulting modification of the ζ potential. Different colors represent the different data sets.

Nevertheless, we cannot exclude other explanations for this effect, i.e.:

(i) carbon dioxide that is solved in water [48]. The carbon dioxide is dissolved in water forming carbonates and hydrocarbonates, i.e. $CO_3^{2-} + H_20 = HCO_3^- + OH^-$. The equilibrium pK of this reaction is at pH of 6.5, which is the value of the maximum of the surface potential rise. Additionally, hydrocarbonates are known to be adsorbed at a variety of different surfaces as it is investigated with e.g. radiotracer [70].
(ii) the plasma activation can also affect the decrease of the ζ potential, however, the effect should not be so strong.

Step C, Citrates: The next process step is the deposition of citrate-stabilized gold nanoparticles onto the APTES layer. The pH dependence of the ζ potential of three samples with different AuNPs densities is presented in Figure 44c. The particle density is investigated by means of SEM and then calculated using an open-source software (ImageJ). Corresponding SEM pictures are shown in Figure 48.

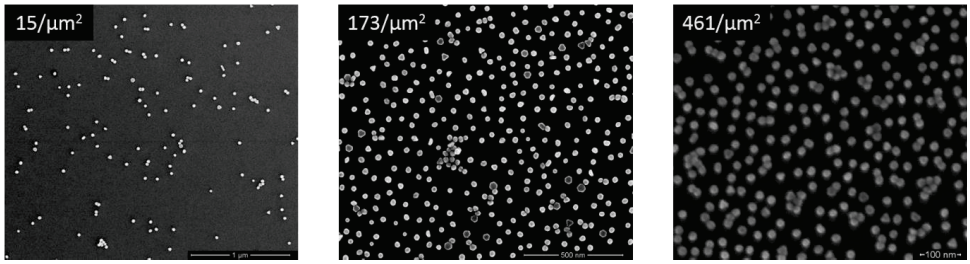

Figure 48: SEM pictures of different density of citrate-stabilized AuNPs on the SiO_2 surface covered with APTES.

The upper curve (green squares) in Figure 44c shows a similar behavior as the freshly measured APTES monolayers (Figure 44b), which were already discussed above. Taking into account that this set of data belongs to the smallest AuNP density (15/µm²), we believe that the behavior of a given curve is dictated by the above-mentioned effect of desorption of APTES molecules from the surface during the measurement. Other curves in Figure 44c, representing samples with larger AuNP densities reveal no minimum in the ζ potential characteristic.

In general, the ζ potential is reduced because of the presence of the citrate molecules (negatively charged functional group) stabilizing AuNPs. Obviously, the IEPs are also reduced and, moreover, they depend on the density of AuNPs on the surface (see Figure 47). The higher is the concentration of gold nanoparticles on the surface the lower is the IEP of this system. The time dependence of the ζ potential for this system (Figure 45, red solid triangles) also shows a decrease in time with a time constant similar to the decrease, observed for APTES. We believe that also this decrease is a reminiscence of the APTES layer and has nothing to do with the citrate-stabilized AuNPs. Desorption of AuNPs would rather lead to an increase of the ζ potential and not a decrease.

Step D, AuNPs: In the next step, the free (not involved in the bonding of AuNPs) organic citrates and APTES molecules are etched away with an oxygen plasma (200W, 2min). This leaves two types of activated surfaces: silicon oxide and hydrophobic, inert gold. Due to the removal of the molecules (these are more positively charged APTES molecules than negatively charged citrates) the ζ potential and consequently the IEPs are reduced. However, the oxygen plasma not only removes the free molecules, it also activates the SiO_2 surface and the Au-surface of the AuNPs. As shown in Sections IV.2 and IV.3, this activation modifies the surface potential but is not stable, especially in an electrolyte. Therefore, the data of this step (pH dependence of the ζ potential in Figure 44d and IEP in Figure 47 scatter strongly.

Step E, Aminothiols: In order to identify molecules that would lead to the highest positively charged AuNP surface, which would be optimal for bio applications, we compared different molecules that could be functionalized onto AuNPs. Since we were motivated by the facilitation of cell adhesion, the buffer solution HBSS (Hank's buffered

salt solution, which is often used in cell culture) is used as working electrolyte in this experiment. The use of HBSS ensures a stable pH of 7.2. Nanoparticles are functionalized with different molecules (positively charged aminothiols and negatively charged carboxylthiols) following step E of the preparation process. The resulting ζ potentials are summarized in Figure 49.

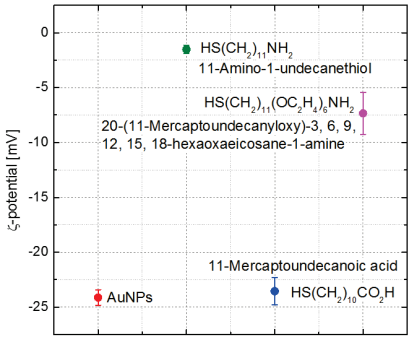

Figure 49: Comparison of the ζ potential at a pH 7.2 (in HBSS as electrolyte) for an activated Si/SiO_2 substrate with AuNPs (step E) functionalized with different molecular monolayers: 11-mercaptoundecanoic acid (blue), 20-(11-mercaptoundecanylocy)-3,6,9,12,15,18-hexaoxaeicosane-1-amine (magenta), and 11-amino-1-undecanethiol (green). Additionally, the ζ potential of the sample (Si/SiO_2 with AuNPs) without functionalization is given.

The ζ potential of the non functionalized sample (Si/SiO_2 with AuNPs) is around -24mV. Only two of the molecules show a significant increase of the ζ potential in HBSS. The strongest increase in observed for 11-amino-1-undecanethiol molecules (green circle), which are simpler and known for their close packing. The second molecule, 20-(11-mercaptoundecanylocy)-3,6,9,12,15,18-hexaoxaeicosane-1-amine (magenta), possesses side chains, which reduce the packing density due to interactions. This automatically leads to a smaller relative value of the ζ potential. Finally, the negatively charged molecules, 11-mercaptoundecanoic acid (blue circle), do not modify the negative charge of the surface significantly. Therefore, the ζ potential is hardly changed for this functionalization.

Due to their higher absolute positive charge at the physiological pH, the 11-amino-1-undecanethiol molecules (abbreviated Aminothiols in the following) are further used for the functionalization of AuNPs. The pH-dependence of the ζ potential of the last process step (deposition of Aminothiols) is shown in Figure 44e. The surfaces of the AuNPs are positively charged, due to the protonation of the amino-groups. The increase of the ζ potential with respect to the previous step D is visible (see Figure 44e), it is smaller compared to step B (deposition of APTES). This is expected, since in this case only a small part of the sample (i.e. the AuNPs) is covered with positively charged thiols, whereas the complete substrate was covered with the silane (APTES) in step B. However, it should be noticed that in this case, the pH dependence is measured after the stability test, shown in Figure 45. The latter actually shows that the ζ potential

measured for the functionalization with Aminothiols is very similar to that of the functionalization of SiO_2 with APTES. In addition, the time dependent reduction of the ζ potential is quite similar. This indicates that maybe the same mechanism is responsible for this behavior, i.e. desorption of molecules or reaction with carbonates.

In summary, we can partially understand the modification and stability of the surface potential of a substrate functionalized with various molecules and AuNPs. The change of the IEP (Figure 47) generally follows the expected change of the surface charge for the different steps.

The total (integral) surface potential depends on all possible charge sources (substrate, AuNPs and molecules) that add to the resulting total charge. Such model might be described by

$$\zeta = \sum_i \zeta_i A_i, \tag{27}$$

where A_i represents the surface of a given type with a potential ζ_i. Similar proposals are presented in [10], [71]. This approach explains, for instance, why the time-dependent ζ potential of positively charged molecular layers still has an impact on the ζ potential measured after the deposition of AuNPs.

Finally, the measurements provide vital information on the stability and reliability of the different process steps (Figure 45). Generally, it seems that both functionalizations with molecules lead to an unstable surface potential. In both cases (the silane APTES and the thiol Aminothiol) the ζ potential strongly decreases due to desorption of these molecules or reaction of the positively charged amino-group with, for instance, hydrocarbonates.

As such, our streaming potential/current technique represents an ideal tool to analyze and monitor the complex surfaces and their modification.

Summary

In the field of bioelectronics the optimization of the interface between cells and substrates plays a major role. It affects the cell adhesion to a substrate, controls the immobilization of neurons and guidance of neurite outgrowths on the surface and can establish a well-defined and stable contact between cells and the substrate's surface in order to get the optimal signal transfer in bioelectronic devices. These challenges are strongly dependent on the surface chemistry, one important aspects of which is the surface charge, caused by the surface nature as well as by specific adsorption from its environment e.g. an electrolyte that is vital for the biological components.

In this dissertation, we tried to demonstrate that the streaming potential/streaming current method is the one of the best methods for investigation of the electric properties of surfaces that can be applied to complex inorganic as well as organic interfaces used for bioelectronic applications. Generally, the surface charging effects not only yield extremely small signals, they are also sensitive to any contamination. It became clear in this work that the quality of the aqueous media as well as the cleanliness of the surface are of great importance in order to perform reliable and reproducible measurements.

During the work, we

(i) developed and tested a setup for the deposition of molecular monolayers, including in-situ cleaning and activation, accompanied by in-situ electronic analysis. Using the deposition device, molecular monolayers of different silanes (1H,1H,2H,2H-perfluorooctyltrichlorosilan (FOTCS) and 3-aminopropyltriethoxysilane (APTES)) are deposited onto various biocompatible substrates. The deposition is monitored via capacitive and microwave measurements, the resulting film is analyzed via ellipsometry and wetting angle measurements. Additionally, the deposition of functionalized AuNPs on the molecular layer is tested.

(ii) improved and optimized a streaming potential/streaming current experiment for the analysis of the surface potential of the substrates and layers. This method is usually used in a qualitative, i.e. comparative way. By introducing various modifications (especially an extensive purging of the electrolyte with N_2) and by optimizing the measuring procedure using an ideal inert and hydrophobic test material (i.e. polypropylene) we could establish a reliable quantitative type of measurement.

With the optimized streaming potential/streaming current technique extensive studies on different classes of surfaces that might be important for bioelectronic applications have been performed, including:

(i) various substrates (i.e. Si, borosilicate glass, and sapphire) in the activated and original form,
(ii) metallic layers (Pt, Au, and for comparison Cr),
(iii) graphene layer on various substrates,
(iv) molecular layers (various silanes and thiols functionalized with positive or negative charge),
(v) Au-nanoparticles, and
(vi) combination of different surfaces listed above.

Using especially the time- and pH-dependent analysis of the ζ potential, we could:

(i) identify possible candidates for the modification of a given surface with respect to their surface potential (e.g. depending on density, stability and functional group, the monolayers of organic molecules can possess different ζ potential)
(ii) determine the stability of a given surface (e.g. time-dependent measurements of ζ potential can reveal the desorption of molecules from the surface or the reconstruction of silanol bonds in-situ)
(iii) identify the surface composition (e.g. using pH-dependent measurements of ζ potential it is possible to determine the chemistry of the surface, including reactive groups, specifically adsorbed ions, etc. depending on the crystal orientation or oxidation of a given sample)
(iv) monitor the change of the surface potential due to the engineering of a surface via deposition of inorganic (e.g. graphene or noble metal), organic layers (silanes and thiols) or nanoparticles (different densities of AuNPs tailored with organic molecules of different charges), or external treatment (e.g. oxidation, annealing or activation of the surface) as well as identify the presence of a contaminant.

Although only a limited number of model systems was discussed, this work demonstrates the potential of studying the electrical properties of surfaces in aqueous solutions. It demonstrates promising perspectives for the construction of robust and reliable devices for molecular electronics, bioelectronics and sensoric, e.g. (IS)FETs, MEAs, supercapacitors and crossbar junctions, as well as for purely biological problems, e.g. understanding, influencing and facilitating of the adhesion as well as guiding of proteins, cells and bacteria on a surface.

References

[1] J. D. Andrade, “Interfacial phenomena and biomaterials,” *Med. Instruments*, vol. 7, no. 2, pp. 110–120, 1973.

[2] N. Faucheux, R. Schweiss, K. Lützow, C. Werner, and T. Groth, “Self-assembled monolayers with different terminating groups as model substrates for cell adhesion studies.,” *Biomaterials*, vol. 25, no. 14, pp. 2721–30, Jun. 2004.

[3] P. Roach, T. Parker, N. Gadegaard, and M. R. Alexander, “Surface strategies for control of neuronal cell adhesion: A review,” *Surf. Sci. Rep.*, vol. 65, no. 6, pp. 145–173, Jun. 2010.

[4] W. Hällström, T. Mårtensson, C. N. Prinz, P. Gustavsson, L. Montelius, L. Samuelson, and M. Kanje, “Gallium phosphide nanowires as a substrate for cultured neurons.,” *Nano Lett.*, vol. 7, no. 10, pp. 2960–5, Oct. 2007.

[5] C. N. Prinz, W. Hällström, T. Mårtensson, L. Samuelson, L. Montelius, and M. Kanje, “Axonal guidance on patterned free-standing nanowire surfaces.,” *Nanotechnology*, vol. 19, no. 34, p. 345101, Aug. 2008.

[6] W. Hällström, C. N. Prinz, D. Suyatin, L. Samuelson, L. Montelius, and M. Kanje, “Rectifying and sorting of regenerating axons by free-standing nanowire patterns: a highway for nerve fibers.,” *Langmuir*, vol. 25, no. 8, pp. 4343–6, Apr. 2009.

[7] N. M. Dowell-Mesfin, M. Abdul-Karim, a M. P. Turner, S. Schanz, H. G. Craighead, B. Roysam, J. N. Turner, and W. Shain, “Topographically modified surfaces affect orientation and growth of hippocampal neurons.,” *J. Neural Eng.*, vol. 1, no. 2, pp. 78–90, Jun. 2004.

[8] F. Santoro, J. Schnitker, G. Panaitov, and A. Offenhäusser, “On chip guidance and recording of cardiomyocytes with 3D mushroom-shaped electrodes.,” *Nano Lett.*, vol. 13, no. 11, pp. 5379–84, Jan. 2013.

[9] P. Bongrand, C. Capo, and R. Depieds, “Physics of cell adhesion,” *Prog. Surf. Sci.*, vol. 12, no. 3, pp. 217–285, Jan. 1982.

[10] A. Carré, V. Lacarrière, and W. Birch, “Molecular interactions between DNA and an aminated glass substrate,” *J. Colloid Interface Sci.*, vol. 260, no. 1, pp. 49–55, Apr. 2003.

[11] C. Werner, “Interfacial phenomena and biomaterials.,” in *Polymer Surfaces and Interfaces*, M. Stamm, Ed. Springer Berlin Heidelberg, 2008, pp. 299–318.

[12] W. Norde and J. Lyklema, “Why proteins prefer interfaces,” *J. Biomater. Sci. Polym. Ed.*, vol. 2, no. 3, pp. 183–202, Jan. 1991.

[13] A. T. Poortinga, R. Bos, W. Norde, and H. J. Busscher, “Electric double layer interactions in bacterial adhesion to surfaces,” *Surf. Sci. Rep.*, vol. 47, no. 1, pp. 1–32, Jun. 2002.

[14] E. Yavin and Z. Yavin, “Attachment and culture of dissociated cells from rat embryo cerebral hemispheres on poly lysine-coated surface,” *J. Cell Biol.*, vol. 62, pp. 540–546, 1974.

[15] M. Matsuzawa, R. S. Potember, D. a Stenger, and V. Krauthamer, “Containment and growth of neuroblastoma cells on chemically patterned substrates.,” *J. Neurosci. Methods*, vol. 50, no. 2, pp. 253–60, Nov. 1993.

[16] M. Matsuzawa, R. S. Potember, and V. Krauthamer, “Use of chemically patterned substrate to study directional effect of damaging electrical stimulation on cultured neuroblastoma cells.,” *Brain Res.*, vol. 667, no. 1, pp. 47–53, Dec. 1994.

[17] P. M. St John, L. Kam, S. W. Turner, H. G. Craighead, M. Issacson, J. N. Turner, and W. Shain, “Preferential glial cell attachment to microcontact printed surfaces.,” *J. Neurosci. Methods*, vol. 75, no. 2, pp. 171–7, Aug. 1997.

[18] S.-J. Yen, W.-L. Hsu, Y.-C. Chen, H.-C. Su, Y.-C. Chang, H. Chen, S.-R. Yeh, and T.-R. Yew, “The enhancement of neural growth by amino-functionalization on carbon nanotubes as a neural electrode.,” *Biosens. Bioelectron.*, vol. 26, no. 10, pp. 4124–32, Jun. 2011.

[19] S. Wall, “The history of electrokinetic phenomena,” *Curr. Opin. Colloid Interface Sci.*, vol. 15, no. 3, pp. 119–124, Jun. 2010.

[20] M. Zembala, “Electrokinetics of heterogeneous interfaces.,” *Adv. Colloid Interface Sci.*, vol. 112, no. 1–3, pp. 59–92, Dec. 2004.

[21] D. C. Grahame, “The Electrical Double Layer and the Theory of Electrocapillarity,” 1947.

[22] A. V. Delgado, F. González-Caballero, R. J. Hunter, L. K. Koopal, and J. Lyklema, “Measurement and interpretation of electrokinetic phenomena.,” *J. Colloid Interface Sci.*, vol. 309, no. 2, pp. 194–224, May 2007.

[23] B. Salopek, D. Krasic, and S. Filipovic, “Measurement and application of zeta-potential,” *Rud. Zb.*, vol. 4, pp. 147–151, 1992.

[24] J. Lyklema, “Surface charges and electrokinetic charges: Distinctions and juxtapositionings,” *Colloids Surfaces A Physicochem. Eng. Asp.*, vol. 376, no. 1–3, pp. 2–8, Feb. 2011.

[25] H.-J. Jacobasch, “Characterization of solid surfaces by electrokinetic measurements,” *Prog. Org. Coatings*, vol. 17, no. 2, pp. 115–133, Jul. 1989.

[26] J. Lyklema, Ed., *Fundamentals of Interfaces and Colloid Science, vol. II*. New York: Academic Press, 1995, p. Chaps. 3, 4.

[27] C. P. Smith and H. S. White, “Voltammetry of Molecular Films Containing Acid/Base Groups,” *Langmuir*, vol. 9, no. 1, 1993.

[28] B. B. Weiner, W. W. Tscharnuter, D. Fairhurst, B. Instruments, C. Holtsville, and N. Y. Us, “Zeta Potential : A New Approach,” in *Canadian Mineral Analysts Meeting*, 1993.

[29] J. Lyklema, “Overcharging, charge reversal: Chemistry or physics?,” *Colloids Surfaces A Physicochem. Eng. Asp.*, vol. 291, no. 1–3, pp. 3–12, Dec. 2006.

[30] M. von Smoluchowski, “Contribution a la theorie de l’endosmose electrique et de quelques phenomenes correlatifs,” *Bull Acad Sci Cracovie Cl. Sci Math Natur*, vol. 182, no. 99, 1903.

[31] L. Romaner, G. Heimel, C. Ambrosch-Draxl, and E. Zojer, “The Dielectric Constant of Self-Assembled Monolayers,” *Adv. Funct. Mater.*, vol. 18, no. 24, pp. 3999–4006, Dec. 2008.

[32] M. Lessel, O. Bäumchen, M. Klos, H. Hähl, R. Fetzer, M. Paulus, R. Seemann, and K. Jacobs, “Self-assembled silane monolayers : An efficient step-by-step recipe for high-quality , low energy surfaces,” 2014.

[33] E. T. Vandenberg, L. Bertilsson, B. Liedberg, K. Uvdal, R. Erlandsson, H. Elwing, and I. Lundström, “Structure of 3-Aminopropyl Triethoxy Silane on Silicon Oxide,” *J. Colloid Interface Sci.*, vol. 147, no. 1, pp. 103–118, 1991.

[34] J. B. Brzoska, I. Ben Azouz, and F. Rondelez, “Silanization of Solid Substrates: A Step Toward Reproducibility,” *Langmuir*, vol. 10, no. 11, pp. 4367–4373, Nov. 1994.

[35] J. C. Love, L. a Estroff, J. K. Kriebel, R. G. Nuzzo, and G. M. Whitesides, *Self-assembled monolayers of thiolates on metals as a form of nanotechnology.*, vol. 105, no. 4. 2005, pp. 1103–69.

[36] I. Batyrev, B. Tuttle, D. Fleetwood, R. Schrimpf, L. Tsetseris, and S. Pantelides, “Reactions of Water Molecules in Silica-Based Network Glasses,” *Phys. Rev. Lett.*, vol. 100, no. 10, p. 105503, Mar. 2008.

[37] H. Neergaard Waltenburg and J. T. Yates, “Surface Chemistry of Silicon,” *Chem. Rev.*, vol. 95, no. 5, pp. 1589–1673, Jul. 1995.

[38] S. Gilles, “Chemical Modification of Silicon Surfaces for the Application in Soft Lithography,” 2011.

[39] M. Arnold, E. A. Cavalcanti-Adam, R. Glass, J. Blümmel, W. Eck, M. Kantlehner, H. Kessler, and J. P. Spatz, “Activation of integrin function by nanopatterned adhesive interfaces.,” *Chemphyschem*, vol. 5, no. 3, pp. 383–8, Mar. 2004.

[40] M. Arnold, V. C. Hirschfeld-Warneken, T. Lohmüller, P. Heil, J. Blümmel, E. A. Cavalcanti-Adam, M. López-García, P. Walther, H. Kessler, B. Geiger, and J. P. Spatz, “Induction of cell polarization and migration by a gradient

of nanoscale variations in adhesive ligand spacing.," *Nano Lett.*, vol. 8, no. 7, pp. 2063–9, Jul. 2008.

[41] E. A. Cavalcanti-Adam, T. Volberg, A. Micoulet, H. Kessler, B. Geiger, and J. P. Spatz, "Cell spreading and focal adhesion dynamics are regulated by spacing of integrin ligands.," *Biophys. J.*, vol. 92, no. 8, pp. 2964–74, Apr. 2007.

[42] M. Arnold, M. Schwieder, J. Blümmel, E. A. Cavalcanti-Adam, M. Lopez-Garcia, H. Kessler, B. Geiger, and J. P. Spatz, "Cell interactions with hierarchically structured nano-patterned adhesive surfaces," *Soft Matter*, vol. 5, pp. 72–77, 2009.

[43] C. Selhuber-Unkel, T. Erdmann, M. López-García, H. Kessler, U. S. Schwarz, and J. P. Spatz, "Cell adhesion strength is controlled by intermolecular spacing of adhesion receptors.," *Biophys. J.*, vol. 98, no. 4, pp. 543–51, Mar. 2010.

[44] S. Gilles, C. Kaulen, M. Pabst, U. Simon, A. Offenhäusser, and D. Mayer, "Patterned self-assembly of gold nanoparticles on chemical templates fabricated by soft UV nanoimprint lithography.," *Nanotechnology*, vol. 22, no. 29, p. 295301, Jul. 2011.

[45] M.-A. Neouze and U. Schubert, "Surface Modification and Functionalization of Metal and Metal Oxide Nanoparticles by Organic Ligands," *Monatshefte für Chemie - Chem. Mon.*, vol. 139, no. 3, pp. 183–195, Feb. 2008.

[46] S. Gilles, S. Winter, K. E. Michael, S. H. Meffert, P. Li, K. Greben, U. Simon, A. Offenhäusser, and D. Mayer, "Control of cell adhesion and neurite outgrowth by patterned gold nanoparticles with tunable attractive or repulsive surface properties.," *Small*, vol. 8, no. 21, pp. 3357–67, Nov. 2012.

[47] V. Belanohava, "Charakterisierung und Oberflächenmodifizierung oxidischer Schichtsysteme für biophysikalische Anwendungen," 2012.

[48] T. Luxbacher, *The ZETA Guide: Principles of the streaming potential technique*, 1st ed. Graz: Anton Paar GmbH, 2014, p. 137.

[49] C. Werner, H. Körber, R. Zimmermann, S. S. Dukhin, and H.-J. Jacobasch, “Extended Electrokinetic Characterization of Flat Solid Surfaces.,” *J. Colloid Interface Sci.*, vol. 208, no. 1, pp. 329–346, Dec. 1998.

[50] C. Bellmann, A. Opfermann, H.-J. Jacobasch, and H.-J. Adler, “Characterisation of pure or coated metal surfaces with streaming potential measurements,” *Fresenius. J. Anal. Chem.*, vol. 358, no. 1–2, pp. 255–258, May 1997.

[51] R. Zimmermann, U. Freudenberg, R. Schweiß, D. Küttner, and C. Werner, “Hydroxide and hydronium ion adsorption — A survey,” *Curr. Opin. Colloid Interface Sci.*, vol. 15, no. 3, pp. 196–202, Jun. 2010.

[52] D. Stawski and C. Bellmann, “Electrokinetic properties of polypropylene textile fabrics containing deposited layers of polyelectrolytes,” *Colloids Surfaces A Physicochem. Eng. Asp.*, vol. 345, no. 1–3, pp. 191–194, Aug. 2009.

[53] H.-J. Jacobasch, K. Grundke, S. Schneider, and F. Simon, “The influence of additives on the adhesion behaviour of thermoplastic materials used in the automotive industry,” vol. 26, no. 95, 1995.

[54] M. Kosmulski, “A literature survey of the differences between the reported isoelectric points and their discussion,” *Colloids Surfaces A Physicochem. Eng. Asp.*, vol. 222, no. 1–3, pp. 113–118, Jul. 2003.

[55] M. Kosmulski, “The pH-dependent surface charging and points of zero charge: V. Update.,” *J. Colloid Interface Sci.*, vol. 353, no. 1, pp. 1–15, Jan. 2011.

[56] R. J. Kershner, J. W. Bullard, and M. J. Cima, “Zeta potential orientation dependence of sapphire substrates.,” *Langmuir*, vol. 20, no. 10, pp. 4101–8, May 2004.

[57] G. V. Franks and L. Meagher, “The isoelectric points of sapphire crystals and alpha-alumina powder,” *Colloids Surfaces A Physicochem. Eng. Asp.*, vol. 214, no. 1–3, pp. 99–110, Mar. 2003.

[58] D. E. Yates and T. W. Healy, “The structure of the silica/electrolyte interface,” *J. Colloid Interface Sci.*, vol. 55, no. 1, pp. 9–19, Apr. 1976.

[59] H. Zhang, A. a Hassanali, Y. K. Shin, C. Knight, and S. J. Singer, “The water-amorphous silica interface: analysis of the Stern layer and surface conduction.,” *J. Chem. Phys.*, vol. 134, no. 2, p. 024705, Jan. 2011.

[60] G. K. Lockwood and S. H. Garofalini, “Bridging oxygen as a site for proton adsorption on the vitreous silica surface.,” *J. Chem. Phys.*, vol. 131, no. 7, p. 074703, Aug. 2009.

[61] G. A. Parks, “The isoelectric points of solid oxides, solid hydroxides, and aqueous hydroxo complex systems,” *Chem. Rev.*, vol. 65 (2), pp. 177–198, 1965.

[62] L. Bousse, S. Mostarshed, B. van der Shoot, N. F. de Rooij, P. Gimmel, and W. Göpel, “Zeta Potential Measurements of Ta2O5 and SiO2 Thin Films,” *J. Colloid Interface Sci.*, vol. 147, no. 1, pp. 22–32, 1991.

[63] Y. Gu and D. Li, “The ζ-potential of glass surface in contact with aqueous solutions,” *J. Colloid Interface Sci.*, vol. 226, no. 2, pp. 328–339, Jun. 2000.

[64] K. Bourikas, C. Kordulis, and A. Lycourghiotis, “The mechanism of the protonation of metal (hydr)oxides in aqueous solutions studied for various interfacial/surface ionization models and physicochemical parameters: a critical review and a novel approach.,” *Adv. Colloid Interface Sci.*, vol. 121, no. 1–3, pp. 111–30, Sep. 2006.

[65] M. Kosmulski, “The pH-dependent surface charging and the points of zero charge.,” *J. Colloid Interface Sci.*, vol. 253, no. 1, pp. 77–87, Sep. 2002.

[66] M. Giesbers, J. M. Kleijn, and M. a Cohen Stuart, “The electrical double layer on gold probed by electrokinetic and surface force measurements.,” *J. Colloid Interface Sci.*, vol. 248, no. 1, pp. 88–95, Apr. 2002.

[67] A. Schrems, A. Kibrom, S. Küpcü, E. Kiene, U. B. Sleytr, and B. Schuster, “Bilayer lipid membrane formation on a chemically modified S-layer lattice.,” *Langmuir*, vol. 27, no. 7, pp. 3731–8, Apr. 2011.

[68] B. J. Kirby and E. F. Hasselbrink, “Zeta potential of microfluidic substrates: 2. Data for polymers.,” *Electrophoresis*, vol. 25, no. 2, pp. 203–13, Jan. 2004.

[69] M. Giesbers, J. M. Kleijn, and M. a Cohen Stuart, “Interactions between acid- and base-functionalized surfaces.,” *J. Colloid Interface Sci.*, vol. 252, no. 1, pp. 138–48, Aug. 2002.

[70] P. Somasundaran, *Encyclopedia of surface and colloid science. 7*, 2nd ed. New York: CRC Press, 2006, pp. 5101–5830.

[71] M. Duc, F. Gaboriaud, and F. Thomas, “Sensitivity of the acid–base properties of clays to the methods of preparation and measurement1. Literature review,” *J. Colloid Interface Sci.*, vol. 289, no. 1, pp. 139–147, Sep. 2005.

Acknowledgements

This dissertation is a short summary of the work, which was conducted in Peter Grünberg Institute/Institute for Complex Systems (PGI-8/ICS-8): Bioelectronics of the Research Center Jülich during my PhD studentship (10.2011-01.2015). In this section I want to cordially acknowledge everyone for the collaboration and enjoyable atmosphere along the entire period of my stay in Jülich.

First of all, I am very grateful to *Prof. Dr. Roger Wördenweber* for being an example of a good scientific practice, leadership and team-organization as well as for being a good phycologist with a sense of humor, for supervising me, for giving me the research freedom and for guiding me during all 5 years of our collaboration, for teaching me how to work effectively, how to organize the entire scientific process, how to work in the multicultural environment and, of course, for being a squash-teammate and mentor.

I show a huge gratitude and appreciation to *Prof. Dr. Vladimir Pan*, who unfortunately passed away in 2013, for giving me an inspiration to start a career in science and for believing in me and giving me an opportunity to work and learn from inside of his group in Institute for Metal Physics in Kyiv in the Department of Superconductivity.

For the organization of the working process, creating a convenient environment in PGI-8/ICS-8 and for supporting my work I acknowledge *Prof. Dr. Andreas Offenhäusser*.

Special thanks is given to *Dr. Eugen Hollmann* for everlasting, honest and genuine interest in my work, for many helpful scientific discussions, for teaching me the sputtering and thin film characterization techniques during my Master work, for technical help with various sample holders during my PhD and for helping and teaching me in the cleanroom as well as for motivating me, making me think and for helping me outside the research center.

I want to show my appreciation to *Dr. Dirk Mayer*, who was my second supervisor during my PhD work, for a number of advices concerning a chemical part of my work, for fruitful discussions and advising me with papers.

I would also like to thank *Prof. Dr. Berenike Maier* for being a second reviewer during my defense phase and *Prof. Dr. Joachim Krug* for chairing.

As many of scientific achievements, my work was based on previous successes of former institute members. For that I am thankful to *Valiantsina Belanohava*, who pioneered the surface potential experiments in our lab and has given me the basis on which I could grow my own work. Although, I haven't personally met *Dr. Sandra Gilles* I thank her very much for the concept and initial tests of CASINO device, which brought us to an exceptional and very promising concept of GLOBUS device as well as for her work with

immobilization and structuring of nanoparticles and cell culture experiments, which was a kick-starting point of our nanoparticle experiments. I want to also show my gratitude to a person, which I never met and, unfortunately, will never have a chance to say my thanks personally to. This is *Dr. Kristin E. Michael*, who unfortunately passed away in 2011 after a short illness, and who showed the importance and potential applicability of the positive surface charges for cell adhesion, which was a starting point of investigations on the electrostatic cell-surface interactions in our institute.

I acknowledge *Pinggui Li* for teaching and helping me with deposition of molecular layers and immobilization of nanoparticles, *Dmitry Kireev* for preparing graphene layers on various substrates for our common experiments and for pushing and motivating me for their characterization. As well I thank *Sung-Eun Choi* for an interest in my results and collaboration concerning surface potential of gold thin films.

Elke Brauweiler-Reuters helped me a lot, spending hours on analyzing my samples with an SEM, *Marco Banzet* has helped me to bring the old oxygen plasma generator back to life and advised me in the cleanroom, together with *Michael Prömpers, Jana Brugger, Iris Klaaßen* and *Jürgen Moers*.

The atmosphere in our group was always outstanding and for that I would like to address a "Kölner" and "Karnevaler" thank to my fellow sufferer *Dr. Thomas Alexander Kurt Grellmann* with whom did we spend about 5 years in the same group in the Research Center and who taught me how to open a bottle of beer with a newspaper and an eye and who contributed much into my knowledge of a German language. I also thank my group members *Tino Ehlig, Yang Dai, Biya Cai* for very friendly atmosphere, for the help with different experiments and in different situations and also for playing chess during the lunch time. I transmit a GLOBUS device to *Aleksandr Markov* and I thank him for our collaborative work on the optimization and electronic detection of organic monolayers as well as for help in the cleanroom. Special thanks is given to *Rolf Kutzner* for the help in construction of devices, for organization of our labs and our work process effectively and for his readiness to help.

For careful support and aspiration to help I am grateful to the electronics team and personally *Stefan Kirch* and *Dipl.Ing. Werner Hürttlen*. For the help in construction and technical issues I am thankful to the workshop team, who made all our ideas on sample holders, devices and constructions become a reality. As well I am thankful to the glass-blowers workshop for producing outstanding GLOBUS as well as a nitrogen purger for my lovely SurPass.

I am very grateful to *Dr. Thomas Luxbacher* and *Dr. Bastian Arlt* from Anton Paar GmbH for advices and hits on working with SurPass and for inviting me to contribute to the seminar on characterization of biomaterials.

I appreciate the time spent in the PGI-8/ICS-8 institute. I have to mention that I am very glad to be a part of this wonderful family and I want to show my gratitude to all

institute members and all my friends outside of the institute although I could forget to thank someone personally.

A huge appreciation, gratitude and love is devoted to my family for enormous support and motivation in my first steps in science during my school and university time, for native love and care and for being proud of me always even when I failed, doubted or couldn't make it.

I want to finish this chapter with showing my gratitude and love to the most important person in my life – my adorable wife Evgenia. I thank her for enormous support during my work, for taking care of me, for listening and finding right words for motivating me, for being herself, for being strong when I was weak, for those beautiful paintings in my office, for inspiration, for help, for many other things and, the most important, for making me happy.

Band / Volume 87
Submolecular imaging with single particle atomic force sensors
G. Kichin (2014), 140 pp
ISBN: 978-3-89336-976-8

Band / Volume 88
Multiscale Multimodel Simulation of Micromagnetic Singularities
C. Andreas (2014), xix, 188 pp
ISBN: 978-3-89336-983-6

Band / Volume 89
***Ab initio* description of transverse transport due to impurity scattering in transition-metals**
B. C. Zimmermann (2014), 164 pp
ISBN: 978-3-89336-985-0

Band / Volume 90
Ladungstransport durch Graphenschichten und GaAs-Nanodrähte untersucht mit einem Multispitzen-Rastertunnelmikroskop
S. Korte (2014), 96 pp
ISBN: 978-3-89336-990-4

Band / Volume 91
6th Georgian-German School and Workshop in Basic Science
A. Kacharava (Ed.) (2014), CD
ISBN: 978-3-89336-991-1

Band / Volume 92
Ab initio investigations of π-conjugated-molecule-metal interfaces for molecular electronics and spintronics
M. Callsen (2014), viii, 155 pp
ISBN: 978-3-89336-992-8

Band / Volume 93
Ladungstransportmessungen an Si(111) Oberflächen mit einem Multispitzen-Rastertunnelmikroskop
M. Blab (2014), iv, 132, X pp
ISBN: 978-3-89336-997-3

Band / Volume 94
Functional Soft Matter
Lecture Notes of the 46th IFF Spring School 2015
23 February – 06 March, 2015 Jülich, Germany
ed. by J. Dhont, G. Gompper, G. Meier, D. Richter, G. Vliegenthart, R. Zorn
(2015), ca. 600 pp
ISBN: 978-3-89336-999-7

Band / Volume 95
2-Steps in 1-pot: enzyme cascades for the synthesis of chiral vicinal amino alcohols
T. Sehl (2014), XIV, 167 pp
ISBN: 978-3-95806-001-2

Band / Volume 96
Immunohistochemical and electrophysiological characterization of the mouse model for Retinitis Pigmentosa, *rd10*
S. Biswas (2014), XII, 119 pp
ISBN: 978-3-95806-011-1

Band / Volume 97
Single molecule localization microscopy: Imaging of cellular structures and a new three-dimensional localization technique
X. Fan (2014), XII, 92 pp
ISBN: 978-3-95806-014-2

Band / Volume 98
Cryogenic Break-Junction Characterization of Single Organic Molecules
T. Grellmann (2014), VI, 86 pp
ISBN: 978-3-95806-015-9

Band / Volume 99
Interacting Interactions: A Study on the Interplay of Molecule-Molecule and Molecule-Substrate Interactions at Metal-Organic Interfaces
M. Willenbockel (2014), IX, 245 pp
ISBN: 978-3-95806-018-0

Band / Volume 100
Microwire crossbar arrays for chemical, mechanical, and thermal stimulation of cells
P. Rinklin (2015), xii, 184 pp
ISBN: 978-3-95806-022-7

Band / Volume 101
Modification and characterization of potential bioelectronic interfaces
K. Greben (2015), 76 pp
ISBN: 978-3-95806-028-9

Weitere ***Schriften des Verlags im Forschungszentrum Jülich*** unter
http://wwwzb1.fz-juelich.de/verlagextern1/index.asp

Schlüsseltechnologien /
Key Technologies
Band / Volume 101
ISBN 978-3-95806-028-9